Journal of Geodesy (1997) 71: 749–767

Journal of Geodesy

Theory of satellite ground-track crossovers

M. C. Kim

Center for Space Research, The University of Texas at Austin, Austin, Texas, 78712-1085, USA
Tel: +1 512 471 8121; fax: +1 512 471 3570; e-mail: mkim@csr.utexas.edu

Received: 19 November 1996 / Accepted: 12 May 1997

Abstract. The fundamental geometry of satellite ground tracks and their crossover problem are investigated. For idealized nominal ground tracks, the geometry is governed by a few constant parameters whose variations lead to qualitative changes in the crossover solutions. On the basis that the theory to locate crossovers has not been studied in sufficient detail, such changes are described in regard to the number of crossover solutions in conjunction with their bifurcations. Employing the spinor algebra as a tool for establishing the ground-track crossing condition, numerical methodologies to locate crossovers appearing in general dual-satellite ground-track configurations are also presented. The methodologies are applied to precisely determined orbital ephemerides of the GEOSAT, ERS-1, and TOPEX/POSEIDON altimeter satellites.

Key words. Satellite · Ground track · Crossover Bifurcation · Spinor

1 Introduction

In the geodetic applications of an artificial satellite as a platform for active remote sensors, associated measurements are frequently sampled along the ground track of the satellite's nadir point, which is also referred to as the subsatellite point. For instance, a satellite-borne altimeter measures the distance between the satellite and its nadir point so that the measurement, called the satellite altimeter range, can be used in the mapping of the physical shape of the mean sea surface (Kim 1993) and in the monitoring of time-varying oceanographics, such as the oceanic tides (Ma et al. 1994), the oceanic eddy variabilities (Shum et al. 1990b), the global mean sea level rise phenomena (Nerem 1995), etc., when the satellite's orbital trajectory is determined by independent tracking to the satellite (Tapley et al. 1994).

The points where the ground track of a satellite intersects itself on the surface of the earth are called (single-satellite) crossover points. When the intersections are from ground tracks of two distinct satellites, these are usually called dual-satellite crossover points. As a means of obtaining relevant measurements at the same geographic location separated in time, crossover points hold a significant usage in satellite geodesy, especially in the realm of satellite oceanography associated with the applications of satellite altimetry. The satellite-altimeter crossover difference, which is defined as the difference in two satellite altimeter ranges interpolated at a crossover point along their respective ground tracks, provides peculiar time-differenced oceanographics. While the altimeter crossover differences have been also used in the evaluation of an altimeter time-tag bias (Schutz et al. 1982), in the refinements of satellite orbits (Cloutier 1983; Sandwell et al. 1986; Born et al. 1986; Moore and Rothwell 1990; Hsu and Geli 1995; Kozel 1995), in the calibration of a gravity field model (Klokocnik and Wagner 1994), in the estimation of the altimeter inferred sea state bias (Gaspar et al. 1994), in the improvement of a planetary topography model (Stottlemyer 1996), etc., the computational efficiency of locating crossovers cannot be overemphasized as one of routine tasks for such a wide range of applications.

Techniques for the determination of crossover locations have been introduced in several studies. For single-satellite crossovers, Hagar (1977) presented a computational flowchart to obtain circular-orbit ground-track crossovers taking into account the secular perturbation effects of the earth's oblateness. Hereinafter such an idealized circular orbit, its geocentric projection onto the surface of a uniformly rotating spherical earth model, and the associated crossover points will be referred to as the nominal orbit, nominal ground track, and nominal crossover points, respectively. As the nominal orbit and its ground track can be effectively described by a few constant parameters, a set of fundamental mathematical relations between the latitude, longitude, and ground-track crossing times can be easily established. Therefore Rowlands (1981) and Shum (1982) presented iterative

positioning of actual single-satellite crossovers starting from nominal crossovers to utilize altimeter crossover differences in their orbit adjustment and determination studies. As also summarized in Schrama (1989) and Spoecker (1991), the general procedure of single-satellite crossover locating has been based on the search for intersections between piecewise ground tracks segmented by ascending and descending passes (i.e., by semirevolutions), and mainly consists of two steps of the prediction of nominal crossovers and the determination of actual crossovers by interpolating discrete subsatellite points projected from satellite trajectories. As well as the actual determination step, the analytical prediction step itself needs numerical iterations due to the inherent transcendental relation between the latitude and the difference of crossing timings as discussed by Colombo (1984). Such a two-step procedure has also been adopted in finding dual-satellite crossovers. For a particular combination of two nominal orbits, Santee (1985) employed spherical triangular models to make an initial guess of simulated dual-satellite nominal crossovers followed by iterative refinements by updating inclinations. More or less general dual-satellite crossover-finding techniques, all based on the semirevolutions search, have been also discussed by Shum et al. (1990a), and by Moore and Ehlers (1993).

Given orbital ephemerides of actual satellites and a proper definition of ground tracks, the crossover locating problem is to determine the ground-track crossing time-tag pairs. Strictly speaking, the solutions are intersections of two unrelated curves. Depending on the relevant orbit geometries, the number of dual-satellite crossovers can be a priori unknown. There can exist more than one intersection (or no intersection) in a semirevolution ground-track pair and therefore one may lose some crossovers at the prediction step. Even for the counting of crossovers in the nominal single-satellite configuration, we found some aspects overlooked in the previous studies. On the basis that the theory to locate crossovers has not been surveyed in sufficient detail and that we need a more systematic approach to the problem, this paper presents both analytical and numerical aspects of locating crossovers in the cases of the general dual-satellite scenario which include the single-satellite cases as a subset. We first investigate the fundamental geometric structure of ground tracks. With some relevant mathematical tools described in the Appendix, we establish the ground-track crossing condition, followed by numerical strategies for finding them. We will provide an answer to the predictability on the number of crossover solutions. With some treatments on the issue of the nadir mapping of satellite ephemerides onto the reference ellipsoid of revolution, actual applications of the developed techniques to the precisely determined orbital ephemerides of the historic GEOSAT and the currently orbiting ERS-1 and TOPEX/POSEIDON altimeter satellites will be also presented.

2 Nominal ground tracks

The ground track of an earth-orbiting artificial satellite is the time-trace of its subsatellite point: a nadir mapping of the satellite's orbital trajectory onto a prescribed earth-surface model such as a reference ellipsoid of revolution (Torge 1991) or a spherical harmonics geoid model (Shum 1982). While definitions of the nadir mapping and the earth surface can be dependent on a specific problem and earth satellites are under the influence of a variety of perturbations, the nominal ground track is appropriate analytically to investigate the fundamental geometry of ground tracks.

In the rotating earth-fixed geocentric equatorial Greenwich-meridional reference frame (hereinafter, the earth-fixed frame), the orbital angular motion of a satellite can be represented by the geocentric unit vector

$$\hat{r} = \frac{\bar{r}}{r} = \frac{1}{r}\begin{Bmatrix} x \\ y \\ z \end{Bmatrix} = \begin{Bmatrix} \cos\phi\cos\lambda \\ \cos\phi\sin\lambda \\ \sin\phi \end{Bmatrix} = \begin{Bmatrix} \cos\tau\cos\vartheta - \cos i\sin\tau\sin\vartheta \\ \cos\tau\sin\vartheta + \cos i\sin\tau\cos\vartheta \\ \sin i\sin\tau \end{Bmatrix} \quad (1)$$

where $\{x, y, z\}$ denotes the Cartesian components of the satellite position vector $\bar{r}$ associated with its geocentric radius r, latitude ϕ, and longitude λ, τ is the argument of latitude and represents the satellite's orbital rotation, ϑ is the longitude of the orbital ascending node measured from the Greenwich meridian and represents the rotation of the satellite's orbital plane with respect to the rotating earth, and i is the inclination of the orbital plane. For a nominal ground track, i becomes constant and the two rotations τ and ϑ become uniform variables resulting in their linear dependence,

$$\vartheta = \lambda_e - q\tau \quad (2)$$

where λ_e represents the longitudinal origin of the nominal ground track, and q denotes the angular velocity ratio between the two uniform rotations. With the linear dependence we can consider τ as a time-like continuously increasing independent variable (the along-track location in the nominal ground track) and ϑ as a dependent variable which is continuously decreasing, as the rotation of any orbital plane with respect to the earth is always westward (i.e., $q > 0$).

Nominal ground tracks are thus on the three-dimensional parametric space of ($0° \le i \le 180°$, $0 < q < \infty$, $0° \le \lambda_e < 360°$). Apart from the longitudinal origin λ_e, the manner in which a nominal ground track is laid down on the spherical earth is primarily dependent on i and q. While i determines the latitudinal bounds of a nominal orbit and its ground track, it is also the parameter to classify conveniently the longitudinal direction of orbital motions. We say that an orbit is posigrade when $0° \le i < 90°$, is retrograde when $90° < i \le 180°$, and is circumpolar when $i = 90°$. However, such a simple classification is valid only when orbits are viewed from the inertial frame. When orbits are viewed from the earth-fixed frame, in which ground tracks are actually depicted, we need careful accounting for the relative rotational motions between the orbital

planes and the earth. For a nominal orbit the relative rotation can be effectively quantified by the parameter q.

To investigate the behavior of a nominal ground track, using Eqs. (1) and (2), we first formulate the spin-axis component velocity of the unit vector $\hat{r}$,

$$\left(\frac{z}{r}\right)' = \phi' \cos\phi = \sin i \cos\tau = \operatorname{sgn}(\cos\tau)\sqrt{\cos^2\phi - \cos^2 i} \tag{3}$$

and the spin-axis component angular momentum,

$$\begin{aligned}\left(\frac{x}{r}\right)\left(\frac{y}{r}\right)' - \left(\frac{y}{r}\right)\left(\frac{x}{r}\right)' &= \lambda' \cos^2\phi \\ &= \cos i - q + q\sin^2 i\left(1 - \cos^2\tau\right) \\ &= \cos i - q\cos^2\phi\end{aligned} \tag{4}$$

where the prime indicates differentiation with respect to τ, and the sgn function takes 1, 0, or -1 depending on the sign of its argument. Equations (3) and (4) can be combined to yield

$$\frac{1}{\cos\phi}\frac{\mathrm{d}\phi}{\mathrm{d}\lambda} = \frac{\pm\sqrt{\cos^2\phi - \cos^2 i}}{\cos i - q\cos^2\phi} \tag{5}$$

which represents the instantaneous slope of the nominal ground track on the unit sphere. Note that for given values of i and q, the slope is a double-valued function of the latitude ϕ.

The latitudinal motion of the nominal ground track is bounded in $\cos\phi \geq |\cos i|$ and is

$$\begin{cases} \text{northward when} & \cos\tau > 0 \\ \text{stationary when} & \cos\tau = 0 \\ \text{southward when} & \cos\tau < 0 \end{cases} \tag{6}$$

as the sign of ϕ' in Eq. (3) will indicate. Meanwhile the longitudinal motion can be somewhat complex. As the sign of λ' in Eq. (4) will indicate, the nominal ground track is

$$\begin{cases} \text{eastward when} & \cos^2\tau < f\left(\cos^2\phi < q^{-1}\cos i\right) \\ \text{stationary when} & \cos^2\tau = f\left(\cos^2\phi = q^{-1}\cos i\right) \\ \text{westward when} & \cos^2\tau > f\left(\cos^2\phi > q^{-1}\cos i\right) \end{cases} \tag{7}$$

where

$$f = 1 - \frac{q - \cos i}{q\sin^2 i} = \frac{(1 - q\cos i)\cos i}{q(1 - \cos i)(1 + \cos i)} \tag{8}$$

is a constant which can be considered as a parametric function of i and q.

Based on Eqs. (7) and (8), in Fig. 1 we classify the longitudinal direction of nominal ground tracks in the two-dimensional parametric space of $(0 < q < \infty,\ -1 \leq \cos i \leq 1)$. There are four regions separated by $q = \cos i\,(f = 1)$, $q\cos i = 1\,(f = 0)$, $\cos i = 0\,(f = 0)$, and surrounded by $\cos i = -1\,(f = -\infty)$, $\cos i = 1$ $(f = \infty$ when $q < 1$, $f = -\infty$ when $q > 1)$, $q = 0$ $(f = -\infty$ when $\cos i < 0$, $f = \infty$ when $\cos i > 0)$, $q = \infty$ $(f = -\cot^2 i)$. In the region $q < \cos i \leq 1$, the associated ground tracks are always eastward $(f > 1)$. In the two regions $q^{-1} < \cos i \leq 1$ and $-1 \leq \cos i < 0$, the associated ground tracks are always westward $(f < 0)$. Hereinafter these two regions are respectively referred to as the posigrade westward region and the retrograde westward region, where the "posigrade" and "retrograde" indicate the longitudinal direction with respect to the inertial frame (the "eastward" and "westward" are used for the earth-fixed frame). In the remaining region of $0 < \cos i < \min\left(q, q^{-1}\right)$ (where $0 < f < 1$), the associated ground tracks change the longitudinal direction; eastward at higher latitudes of $\cos^2\phi < q^{-1}\cos i$ and westward at lower latitudes of $\cos^2\phi > q^{-1}\cos i$. We will refer to this region as the eastward/westward mixed region or simply the mixed region. It can be said that ground tracks of all circumpolar orbits $(\cos i = 0)$ are westward $(\lambda' = -q < 0)$. The point $q = \cos i = 1$ $(f = 1/2$ as a limit) corresponds to the geostationary orbit whose ground track is motionless over a point on the equator $(\phi \equiv 0,\ \lambda \equiv \lambda_e)$.

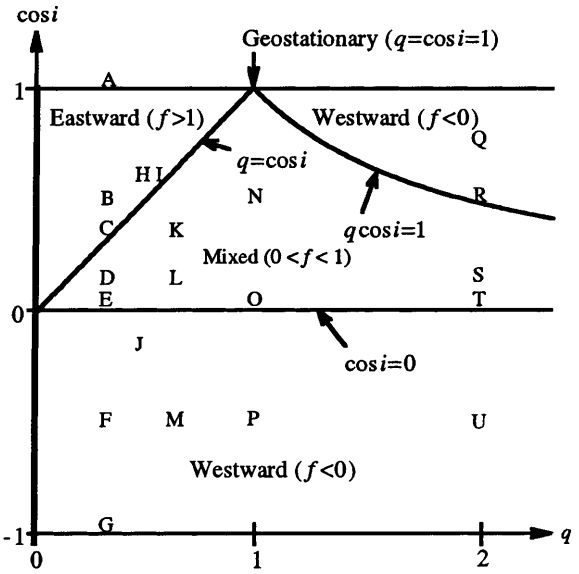

Fig. 1. Longitudinal direction of nominal ground tracks classified in $(q, \cos i)$ space

A nominal ground track will eventually be parallel to its preceding trace with an offset less than some preset limit. To this extent all nominal ground tracks are repeating, although the repeat interval may be as long as possible. Hence we restrict our interest to the cases where q is a rational number, i.e.,

$$q = N/M \tag{9}$$

where M and N are positive coprime integers. With Eq. (9), which is a resonance condition between τ and ϑ, the nominal ground track becomes periodic and repeats its trace after M orbital revolutions of the satellite, or equivalently, N nodal days. In order to visualize the topological evolution of nominal ground tracks, in Fig. 2 we geographically display 21 nominal ground tracks

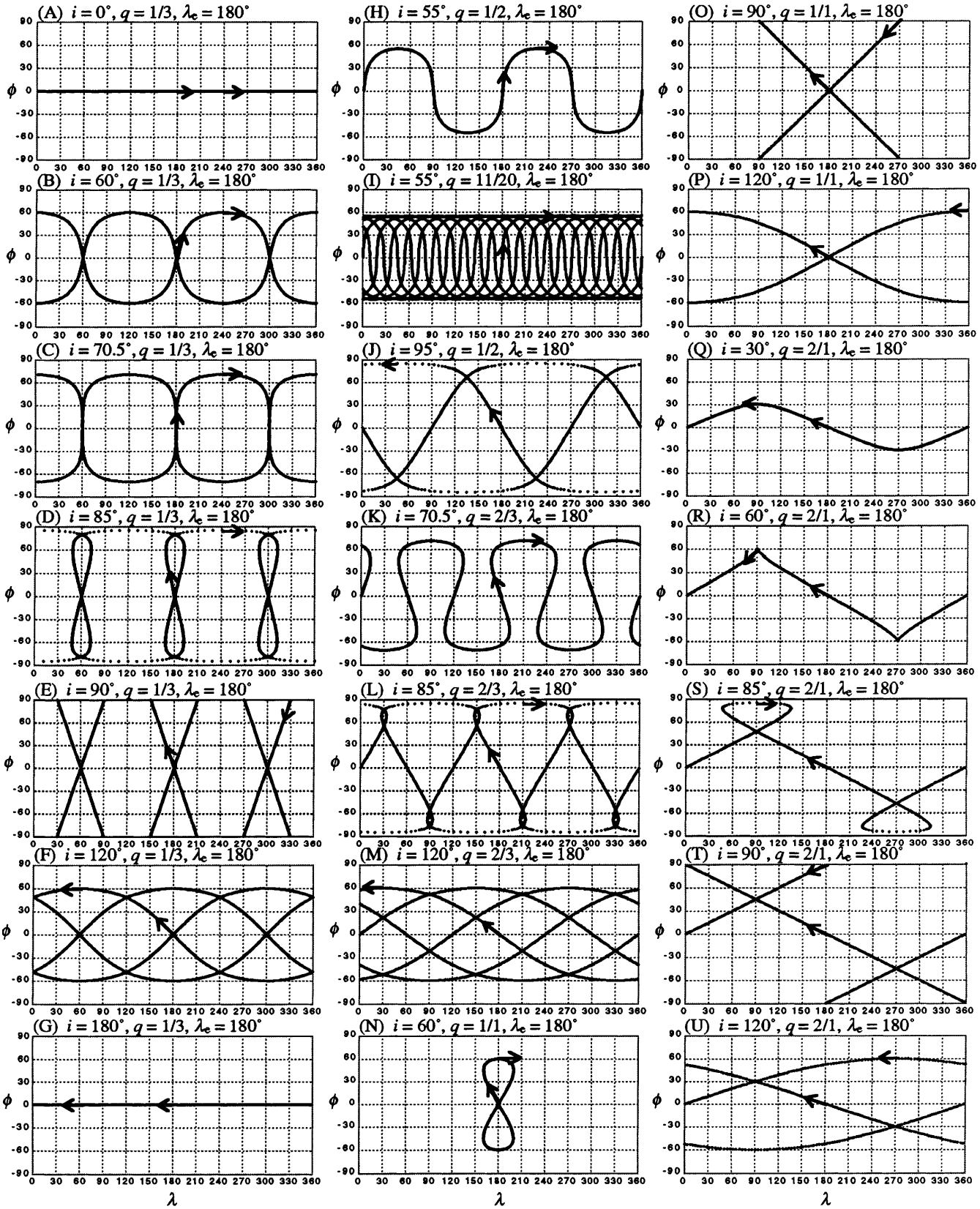

Fig. 2. Nominal ground tracks

(A to U) with the same value of $\lambda_e = 180°$ but with varying q and i as indicated by the corresponding 21 points (A to U) in the $(q, \cos i)$ space shown in Fig. 1. The two arrows in each of the nominal ground tracks indicate the subsatellite point at the epoch ($\tau = 0$) and after a quarter orbital revolution ($\tau = \pi/2$). As the tracks are periodic, we can limit our interest in a repeat period ($0 \leq \tau < 2M\pi$).

The first seven tracks (A–G) correspond to $q = N/M = 1/3$ but with varying i. A($i = 0°$ or $\cos i = 1$) is an eastward equatorial track. In the period of the three (M) orbital revolutions, the track makes two ($M - N$) eastward equatorial revolutions with the net effects of one westward ($-N$) revolution of the orbital node with respect to the earth. As a degenerate case, the track is confined to the equator, and one can say that its actual repeat period is not three (M) revolutions but one and half, i.e., $M/(M - N)$, revolutions. B($i = 60°$ or $\cos i = 1/2$) is a typically inclined eastward ground track. One can say that the two longitudinal revolutions of the track A have been separated with an equatorial symmetry. Now the repeat period becomes three (M) orbital revolutions. There are three crossover points (at the equator) where the two longitudinal revolutions intersect each other. C($i = 70.5°$ or $\cos i = 1/3$) is at the border ($q = \cos i$) of the purely eastward region and the eastward/westward mixed region shown in Fig. 1. The track crosses the equator vertically so that the angle between ascending and descending traces becomes 180° at the crossover points. With D($i = 85°$ or $\cos i \approx 0.087$) we are now in the mixed region. The track is eastward (resp. westward) above (resp. below) $|\phi| \approx 59.2°$, at which it becomes instantaneously meridional ($\lambda' = 0$). There exist nine crossovers with the appearance of six nonequatorial crossovers whose longitudes are aligned with those of equatorial crossovers. E($i = 90°$ or $\cos i = 0$) is a circumpolar ground track which consists of inclined straight lines as both the latitude and longitude become linear functions of τ, i.e., $\phi' \equiv \text{sgn}(\cos \tau)$ and $\lambda' \equiv -q$. Each of the north and south poles becomes a collocation point of three crossovers, and we therefore still have nine crossovers. With F($i = 120°$ or $\cos i = -1/2$) we are now in the retrograde westward region. While there still exist nine crossover points, the longitudes of nonequatorial crossover points are no more aligned with those of the equatorial crossover points. As the last example of $q = 1/3$ cases, G($i = 180°$ or $\cos i = -1$) is a westward equatorial track. Like the track A, the ground-track configuration is again confined to the equator. In the period of the three (M) orbital revolutions the track makes four ($M + N$) westward equatorial revolutions and one can say that its actual repeat period is 3/4, i.e., $M/(M + N)$, revolutions. The equatorial tracks ($\cos i = \pm 1$) actually form degenerate cases, for which the ground-track motion becomes one dimensional.

The next six tracks (H–M) are examples of equatorially asymmetric ground tracks characterized by the opposite parity of M and N. While H($q = 1/2$, $i = 55°$) closely corresponds to a ground track of the Global Positioning System (GPS) satellites (Leick 1995) which generate no crossovers, its neighboring track I($q = 11/20$, $i = 55°$) has 160 crossovers showing the effect of a small change in the value of q. J($q = 1/2$, $i = 95°$) is a highly inclined westward track which shows four crossover points. The following three tracks (K, L, M) are for the same value of $q = 2/3$ but with varying i. While both K($i = 70.5°$) and L($i = 85°$) are located in the mixed region, they are quite different as far as the number of crossovers is concerned; none in K and twelve in L. The track M($i = 120°$) is another typical westward track having the same number of crossovers as L but with a quite different topological structure.

The next three tracks (N, O, P) correspond to $q = 1/1$. N($i = 60°$) is a typical geosynchronous satellite ground track which forms a figure-eight curve. The track librates both latitudinally and longitudinally spending 12 h successively in each of its northern and southern loops. With $q = 1/1$, this geosynchronous behavior is preserved between the geostationary case ($i = 0°$) and the circumpolar geosynchronous case ($i = 90°$) which is shown as the track O. As the track becomes purely retrograde westward ($i > 90°$), the longitude no more librates but undergoes smooth rotations as shown in the track P($i = 120°$). Each of the three tracks has only one crossover point (as its epoch position).

The last five tracks (Q–U) are for $q = 2/1$ but with varying i. With the track Q($i = 30°$) we are now in the posigrade westward region. The track generates no crossover point. R($i = 60°$), a cuspidal track, is a limiting case located at the border ($q \cos i = 1$) of the mixed region and the posigrade westward region. We see two cusps where the ground-track velocity instantaneously becomes zero. With the track S($i = 85°$), we are again in the mixed region showing a looping ground track with an equatorial asymmetry. The cusps of R have been evolved into loops with the appearance of two crossovers. Following another circumpolar track T with two crossover points, the nominal ground track becomes westward again as shown in the track U($i = 120°$).

While all nominal ground tracks have longitudinal cyclic symmetry (i.e., the same pattern repeats M times), they also have either a symmetry or an asymmetry with respect to the equator. The equatorial symmetry occurs when M and N have the same parity (both odd) and the equatorial asymmetry occurs when M and N have the opposite parity. While one can count M equatorial crossovers in the same parity cases, no equatorial crossover point exists in the opposite parity cases due to the asymmetry. In its repeat period, a nominal ground track undergoes M latitudinal librations such that it crosses a zonal line, in $|\sin \phi| < \sin i$, $2M$ times (along each of its M ascending and M descending traces). Meanwhile the longitudinal behavior can be diverse. In case of a retrograde westward track, there are $M + N$ longitudinal revolutions which consist of M revolutions due to the satellite's orbital motion and N revolutions due to the net effects of the orbital plane's motion with respect to the earth. Such a track crosses a meridional line $M + N$ times. Since the $M + N$ longitudinal revo-

lutions interweave so that there exist $M+N-1$ crossover latitudes and each of the crossover latitudes contains M crossover points, the number of crossovers is $M(M+N-1)$. In case of a purely eastward track, there exist $M-N$ longitudinal revolutions which produce $M-N-1$ crossover latitudes and consequently $M(M-N-1)$ crossovers. In case of a posigrade westward track, there exist $N-M$ longitudinal revolutions which produce $N-M-1$ crossover latitudes and consequently $M(N-M-1)$ crossovers. For the eastward/westward mixed tracks, as will be verified later, the number of crossover latitudes varies between $||M-N|-1|$ and $M+N-1$ depending on the values of $\cos i$ and q, and consequently the number of crossovers varies from $M||M-N|-1|$ to $M(M+N-1)$ with the increment M.

Some previous studies have also presented formulas to count the number of single-satellite nominal crossovers appearing in a repeat period. Tai and Fu (1986) claimed that the number equals $M(M-N+1)$ if $\cos i > 0$ and equals $M(M+N-1)$ if $\cos i < 0$ (note that M and N change their notational roles in Tai and Fu). Spoecker (1991) claimed M^2. Considering the case $q < 1$, Cui and Lelgemann (1992) claimed $M(M-\sigma N-1)$ where $\sigma = \mathrm{sgn}(\cos i)$. Along with a sign error in Tai and Fu, and the complete ignorance of the earth rotation effects in Spoecker, these studies passed over the fact that the crossing geometry of a single-satellite nominal ground track is more significantly variant in the two-dimensional parametric space of $(q, \cos i)$. The reciprocal of q has been called the ground-track parameter. Although some of its important roles have been recognized in the counting of crossover latitudes (King 1976; Farless 1985; Parke et al. 1987), we claim that all of these previous studies missed the existence of the eastward/westward mixed tracks and the posigrade westward tracks.

In Fig. 3 we overlay a pair of nominal ground tracks with $(i_1 = 60^\circ, q_1 = 1/3, \lambda_{e1} = 180^\circ)$ and $(i_2 = 95^\circ, q_2 = 1/2, \lambda_{e2} = 155^\circ)$. In addition to the three crossovers of the eastward track and the four crossovers of the westward track, one can count ten points where the two tracks intersect. These intersections, ordered from 1 to 10 along the eastward track, are nominal examples of the dual-satellite crossover point. To fully classify dual-satellite nominal ground-track configurations, one may need to survey a five-dimensional parametric space of $(i_1, i_2, q_1 = N_1/M_1, q_2 = N_2/M_2, \Delta = \lambda_{e1} - \lambda_{e2})$. Here Δ represents the mutual longitudinal origin of two ground tracks, and is introduced to reduce the number of parameters (from six to five) by using the fact that the relative geometry of two nominal ground tracks is invariant upon a simultaneous rotation around a fixed axis. In Sect. 4 we will provide a more systematic treatment for the count of crossovers in both the single- and dual-satellite nominal ground-track configurations.

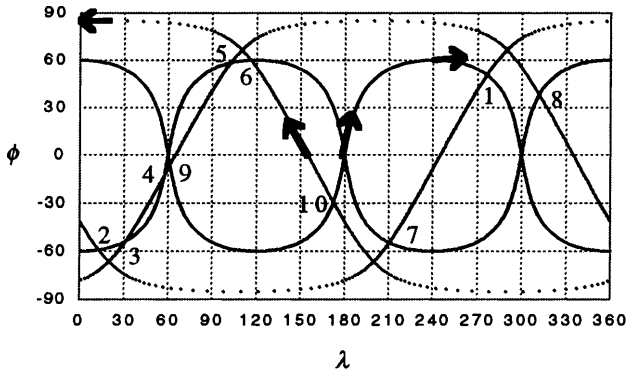

Fig. 3. Overlay of two nominal ground tracks

3 Ground-track intersection

Let $\bar{r}_1(t_1)$ and $\bar{r}_2(t_2)$ be two arbitrary orbital trajectories referenced to the earth-fixed frame, where t_1 and t_2 are time-tags (to be frequently omitted) used as independent variables of the two trajectories. To the extent that the geocentric nadir mapping is concerned, the ground-track crossing condition for the two trajectories can be simply written as

$$\hat{r}_1(t_1) = \hat{r}_2(t_2) \tag{10}$$

where $\hat{r}_1$ and $\hat{r}_2$ are geocentric unit vectors pointing $\bar{r}_1$ and $\bar{r}_2$, respectively.

Let F denote the direction cosine between $\bar{r}_1$ and $\bar{r}_2$, i.e.,

$$F(t_1, t_2) = \cos\psi(t_1, t_2) = \hat{r}_1(t_1) \cdot \hat{r}_2(t_2) \tag{11}$$

where ψ represents the spherical angular distance between the two ground tracks. Locating ground-track crossovers can be considered as a two-dimensional root-finding problem of a single scalar equation $F(t_1, t_2) = 1$, which replaces the vector equation in Eq. (10). Since F yields its maximal value 1 at crossovers, the problem can be solved by using the extremal condition

$$F_{t_1} = \dot{\hat{r}}_1 \cdot \hat{r}_2 = 0, \quad F_{t_2} = \hat{r}_1 \cdot \dot{\hat{r}}_2 = 0 \tag{12}$$

where the subscripts t_1 and t_2 indicate partial differentiations. Given a $\{t_1, t_2\}$ point close to a crossover solution, the Newton-Raphson iteration scheme

$$\begin{Bmatrix} t_1 \\ t_2 \end{Bmatrix} \leftarrow \begin{Bmatrix} t_1 \\ t_2 \end{Bmatrix} - \begin{bmatrix} \ddot{\hat{r}}_1 \cdot \hat{r}_2 & \dot{\hat{r}}_1 \cdot \dot{\hat{r}}_2 \\ \dot{\hat{r}}_1 \cdot \dot{\hat{r}}_2 & \hat{r}_1 \cdot \ddot{\hat{r}}_2 \end{bmatrix}^{-1} \begin{Bmatrix} \dot{\hat{r}}_1 \cdot \hat{r}_2 \\ \hat{r}_1 \cdot \dot{\hat{r}}_2 \end{Bmatrix} \tag{13}$$

may converge to the solution. The iteration fails when the determinant of the 2×2 Hessian matrix, i.e., the Gaussian curvature of F,

$$G = F_{t_1 t_1} F_{t_2 t_2} - F_{t_1 t_2}^2 = \left(\ddot{\hat{r}}_1 \cdot \hat{r}_2\right)\left(\hat{r}_1 \cdot \ddot{\hat{r}}_2\right) - \left(\dot{\hat{r}}_1 \cdot \dot{\hat{r}}_2\right)^2 \tag{14}$$

vanishes.

Let Λ be the angle between $\dot{\hat{r}}_1$ and $\dot{\hat{r}}_2$, i.e.,

$$\dot{\hat{r}}_1 \cdot \dot{\hat{r}}_2 = \left|\dot{\hat{r}}_1\right|\left|\dot{\hat{r}}_2\right| \cos\Lambda \tag{15}$$

At a crossover point, $\hat{r}_1 = \hat{r}_2$, using the relation $\ddot{\hat{r}} \cdot \hat{r} = -\left|\dot{\hat{r}}\right|^2$, Eq. (14) yields

$$G_\chi = \left|\dot{\hat{r}}_1\right|^2\left|\dot{\hat{r}}_2\right|^2 - (\dot{\hat{r}}_1 \cdot \dot{\hat{r}}_2)^2 = \left|\dot{\hat{r}}_1\right|^2\left|\dot{\hat{r}}_2\right|^2 \sin^2\Lambda \tag{16}$$

where the subscript χ, to be frequently omitted on the right-hand sides of equations, indicates evaluation at the crossover point. We note that the iteration failure occurs when the ground tracks become collinear ($\Lambda = 0^\circ$ or 180°).

A converged solution of Eq. (13) does not always yield a crossover solution (where $F = 1$, a maximum of F, or equivalently $\psi = 0$, a minimum of ψ) since other types of extrema also satisfy Eq. (12). In other words, Eq. (12) forms only a necessary condition for a crossover. Figure 4 shows the variation of ψ in the two-dimensional domain $(0 \le \tau_1/2\pi < M_1 = 3,\ 0 \le \tau_2/2\pi < M_2 = 2)$ associated with the two nominal ground tracks shown in Fig. 3. Among the 14 minimal points of ψ in the white area, 10 points correspond to crossovers which are numbered from 1 to 10, consistent with Fig. 3. The remaining four minima labeled by L are local minima. One may also count 14 maxima in the gray area. There actually exist 56 extremal points including 14 saddle points in each of the white and gray areas. The extrema of F can be classified as

$$\text{Extrema}(\nabla F = 0)\begin{cases}\text{Centers}(G>0)\begin{cases}\text{Maxima}(H<0)\begin{cases}\text{Crossovers}(F=1)\\ \text{Local Maxima}(F<1)\end{cases}\\ \text{Minima}(H>0)\end{cases}\\ \text{Saddles}(G<0)\end{cases} \tag{17}$$

where H denotes the mean curvature of F given by $H = (F_{t_1t_1} + F_{t_2t_2})/2$. With the iteration scheme, Eq. (13), we need to check whether a converged solution is a crossover or not. With the symmetry in the numbers of centers and saddles, the symmetry in the numbers of maxima and minima, and the existence of local maxima, less than a quarter of converged solutions will be crossovers.

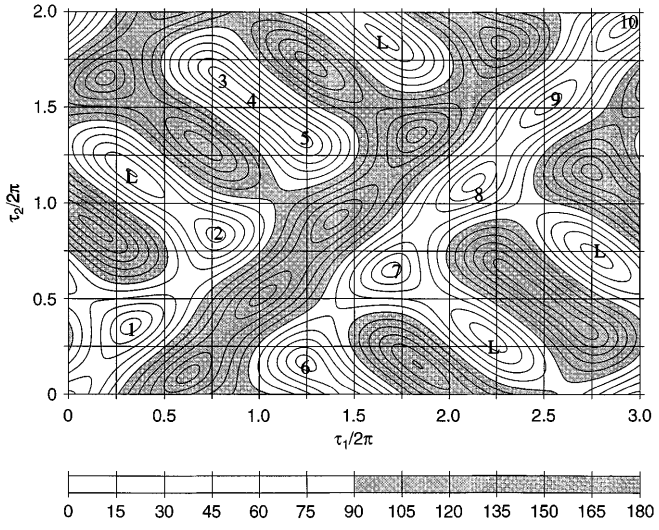

Fig. 4. Spherical angular distance (in degree) between two nominal ground tracks

Now we present an alternative approach by representing the orbital states of satellites in terms of spinors, which enable us to rewrite the ground-track crossing condition in a more convenient form. At this point, the author encourages the reader to refer to the Appendix, which presents a summary on spinors, their algebra, and the two-way transformations between the vector state and the spinor state. Some equations in the Appendix, e.g., the spinor multiplication laws in Eq. (A1), will be frequently used in the following development.

Let $\{\hat{e}_x, \hat{e}_y, \hat{e}_z\}$ be a right-handed orthogonal triad of unit vectors and suppose it forms the earth-fixed frame. We consider the spinor decomposition of the two orbital position vectors

$$\bar{r}_1 = \overline{R}_1^\dagger \hat{e}_x \overline{R}_1, \qquad \bar{r}_2 = \overline{R}_2^\dagger \hat{e}_x \overline{R}_2 \tag{18}$$

with

$$\begin{aligned}\overline{R}_1 &= a_1 + j\left(b_1\hat{e}_x + c_1\hat{e}_y + d_1\hat{e}_z\right)\\ \overline{R}_2 &= a_2 + j\left(b_2\hat{e}_x + c_2\hat{e}_y + d_2\hat{e}_z\right)\end{aligned} \tag{19}$$

where $\{a_1, b_1, c_1, d_1\}$ and $\{a_2, b_2, c_2, d_2\}$ denote the real components of the spinors $\overline{R}_1$ and $\overline{R}_2$ respectively, j is the unit imaginary number, and the superscript $\dagger$ denotes the spinor conjugate.

With Eq. (18) the ground-track crossing condition Eq. (10) can be rewritten as

$$\frac{\overline{R}_1^\dagger \hat{e}_x \overline{R}_1}{r_1} = \frac{\overline{R}_2^\dagger \hat{e}_x \overline{R}_2}{r_2} \tag{20}$$

where, for the magnitudes of the two vectors, we have

$$r_1 = \overline{R}_1^\dagger \overline{R}_1 = \overline{R}_1 \overline{R}_1^\dagger, \qquad r_2 = \overline{R}_2^\dagger \overline{R}_2 = \overline{R}_2 \overline{R}_2^\dagger \tag{21}$$

Premultiplying $\overline{R}_1$ and postmultiplying $\overline{R}_2^\dagger$, Eq. (20) yields

$$\hat{e}_x \overline{R}_1 \overline{R}_2^\dagger = \overline{R}_1 \overline{R}_2^\dagger \hat{e}_x \tag{22}$$

on using Eq. (21).

We introduce a new spinor

$$\overline{Q} = \overline{R}_1 \overline{R}_2^\dagger = A + j\left(B\hat{e}_x + C\hat{e}_y + D\hat{e}_z\right) \tag{23}$$

Substituting Eq. (19) into the product in $\overline{R}_1 \overline{R}_2^\dagger$ in Eq. (23), which is also given in Eq. (A5), one obtains

$$
\begin{aligned}
A &= a_1a_2 + b_1b_2 + c_1c_2 + d_1d_2 \\
B &= b_1a_2 - a_1b_2 - d_1c_2 + c_1d_2 \\
C &= c_1a_2 + d_1b_2 - a_1c_2 - b_1d_2 \\
D &= d_1a_2 - c_1b_2 + b_1c_2 - a_1d_2
\end{aligned} \tag{24}
$$

With Eq. (23), Eq. (22) yields

$$
\hat{e}_x\overline{R}_1\overline{R}_2^{\dagger} - \overline{R}_1\overline{R}_2^{\dagger}\hat{e}_x = \hat{e}_x\overline{Q} - \overline{Q}\hat{e}_x = 2\left(D\hat{e}_y - C\hat{e}_z\right) = 0 \tag{25}
$$

on using Eq. (A1). Note that the ground-track crossing condition is now reduced to

$$
C(t_1, t_2) = 0, \qquad D(t_1, t_2) = 0 \tag{26}
$$

whereas A and B can be arbitrary.

We will refer to the two scalar equations in Eq. (26) as the spinor representation of the ground-track crossing condition. In the (t_1, t_2) domain the crossovers are located at the intersections of the two nonlinear curves; i.e., we are again working with a two-dimensional root-finding problem for a set of the unknown crossover time pairs. The two equations in Eq. (26) can be solved with the Newton- Raphson iteration scheme

$$
\begin{Bmatrix} t_1 \\ t_2 \end{Bmatrix} \leftarrow \begin{Bmatrix} t_1 \\ t_2 \end{Bmatrix} - \begin{bmatrix} C_{t_1} & C_{t_2} \\ D_{t_1} & D_{t_2} \end{bmatrix}^{-1} \begin{Bmatrix} C \\ D \end{Bmatrix} \tag{27}
$$

with

$$
\begin{aligned}
C_{t_1} &= \dot{c}_1a_2 + \dot{d}_1b_2 - \dot{a}_1c_2 - \dot{b}_1d_2 \\
C_{t_2} &= c_1\dot{a}_2 + d_1\dot{b}_2 - a_1\dot{c}_2 - b_1\dot{d}_2 \\
D_{t_1} &= \dot{d}_1a_2 - \dot{c}_1b_2 + \dot{b}_1c_2 - \dot{a}_1d_2 \\
D_{t_2} &= d_1\dot{a}_2 - c_1\dot{b}_2 + b_1\dot{c}_2 - a_1\dot{d}_2
\end{aligned} \tag{28}
$$

obtained on differentiating the last two equations in Eq. (24). It is quite noteworthy that the condition of Eq. (26) is necessary and sufficient, and therefore a converged solution of the spinor-version iteration scheme Eq. (27) always yields a crossover, in contrast to the vector-version iteration scheme of Eq. (13). Equation (27) fails when the determinant of the 2×2 Jacobian matrix,

$$
J = C_{t_1}D_{t_2} - D_{t_1}C_{t_2} \tag{29}
$$

i.e., the Jacobian of the crossing condition Eq. (26), vanishes.

To further analyze the Jacobian, we take partial derivatives of $\overline{Q}$ in Eq. (23), i.e.,

$$
\begin{aligned}
\overline{Q}_{t_1} &= \dot{\overline{R}}_1\overline{R}_2^{\dagger} = A_{t_1} + j\left(B_{t_1}\hat{e}_x + C_{t_1}\hat{e}_y + D_{t_1}\hat{e}_z\right) \\
\overline{Q}_{t_2} &= \overline{R}_1\dot{\overline{R}}_2^{\dagger} = A_{t_2} + j\left(B_{t_2}\hat{e}_x + C_{t_2}\hat{e}_y + D_{t_2}\hat{e}_z\right)
\end{aligned} \tag{30}
$$

For the derivatives $\dot{\overline{R}}_1$ and $\dot{\overline{R}}_2^{\dagger}$, from Eqs. (A44) and (A45), we have

$$
\dot{\overline{R}}_1 = \tfrac{1}{2}\overline{F}_1\overline{R}_1, \ \dot{\overline{R}}_2^{\dagger} = \tfrac{1}{2}\overline{R}_2^{\dagger}\overline{F}_2^{\dagger} \tag{31}
$$

with

$$
\overline{F}_1 = \frac{\dot{r}_1}{r_1} + j\left(\frac{g_1}{r_1^2}\hat{e}_z + \ddot{m}_1\frac{r_1}{g_1}\hat{e}_x\right), \ \overline{F}_2^{\dagger} = \frac{\dot{r}_2}{r_2} - j\left(\frac{g_2}{r_2^2}\hat{e}_z + \ddot{m}_2\frac{r_2}{g_2}\hat{e}_x\right) \tag{32}
$$

where g's are the magnitudes of the total angular momenta,

$$
\begin{aligned}
\overline{g}_1 &= g_1\hat{g}_1 = \overline{r}_1 \times \dot{\overline{r}}_1 = r_1^2\hat{r}_1 \times \dot{\hat{r}}_1 \\
\overline{g}_2 &= g_2\hat{g}_2 = \overline{r}_2 \times \dot{\overline{r}}_2 = r_2^2\hat{r}_2 \times \dot{\hat{r}}_2
\end{aligned} \tag{33}
$$

and $\ddot{m}$'s are the effective normal perturbations of the satellites in the earth-fixed frame.

Substituting Eq. (31) into Eq. (30), we have

$$
\begin{aligned}
\overline{Q}_{t_1} &= \tfrac{1}{2}\overline{F}_1\overline{R}_1\overline{R}_2^{\dagger} = \tfrac{1}{2}\overline{F}_1\overline{Q} \\
\overline{Q}_{t_2} &= \overline{R}_1\tfrac{1}{2}\overline{R}_2^{\dagger}\overline{F}_2^{\dagger} = \tfrac{1}{2}\overline{Q}\,\overline{F}_2^{\dagger}
\end{aligned} \tag{34}
$$

Now, substituting Eq. (32) into Eq. (34), in comparison with Eq. (30), we obtain

$$
\begin{aligned}
A_{t_1} &= \frac{1}{2}\left(\frac{\dot{r}_1}{r_1}A - \frac{g_1}{r_1^2}D - \ddot{m}_1\frac{r_1}{g_1}B\right) \\
B_{t_1} &= \frac{1}{2}\left(\frac{\dot{r}_1}{r_1}B + \frac{g_1}{r_1^2}C + \ddot{m}_1\frac{r_1}{g_1}A\right) \\
C_{t_1} &= \frac{1}{2}\left(\frac{\dot{r}_1}{r_1}C - \frac{g_1}{r_1^2}B + \ddot{m}_1\frac{r_1}{g_1}D\right) \\
D_{t_1} &= \frac{1}{2}\left(\frac{\dot{r}_1}{r_1}D + \frac{g_1}{r_1^2}A - \ddot{m}_1\frac{r_1}{g_1}C\right)
\end{aligned} \tag{35}
$$

and

$$
\begin{aligned}
A_{t_2} &= \frac{1}{2}\left(\frac{\dot{r}_2}{r_2}A + \frac{g_2}{r_2^2}D + \ddot{m}_2\frac{r_2}{g_2}B\right) \\
B_{t_2} &= \frac{1}{2}\left(\frac{\dot{r}_2}{r_2}B + \frac{g_2}{r_2^2}C - \ddot{m}_2\frac{r_2}{g_2}A\right) \\
C_{t_2} &= \frac{1}{2}\left(\frac{\dot{r}_2}{r_2}C - \frac{g_2}{r_2^2}B + \ddot{m}_2\frac{r_2}{g_2}D\right) \\
D_{t_2} &= \frac{1}{2}\left(\frac{\dot{r}_2}{r_2}D - \frac{g_2}{r_2^2}A - \ddot{m}_2\frac{r_2}{g_2}C\right)
\end{aligned} \tag{36}
$$

as similar to Eq. (A34).

With Eqs. (35) and (36), at crossovers, where $C = D = 0$, the Jacobian in Eq. (29) becomes

$$
J_\chi = \frac{1}{2}\frac{g_1}{r_1^2}\frac{g_2}{r_2^2}AB \tag{37}
$$

which, as will be verified, vanishes when the ground tracks become collinear in accordance with G_χ in Eq. (16).

We consider the two rotating satellite-fixed orbital frames (relative to the rotating earth-fixed frame);

$$
\begin{Bmatrix} \hat{r}_1 \\ \hat{g}_1 \times \hat{r}_1 \\ \hat{g}_1 \end{Bmatrix} = \frac{1}{r_1}\overline{R}_1^{\dagger}\begin{Bmatrix} \hat{e}_x \\ \hat{e}_y \\ \hat{e}_z \end{Bmatrix}\overline{R}_1, \ \begin{Bmatrix} \hat{r}_2 \\ \hat{g}_2 \times \hat{r}_2 \\ \hat{g}_2 \end{Bmatrix} = \frac{1}{r_2}\overline{R}_2^{\dagger}\begin{Bmatrix} \hat{e}_x \\ \hat{e}_y \\ \hat{e}_z \end{Bmatrix}\overline{R}_2 \tag{38}
$$

The spinor algebra enables us to write

$$\hat{g}_1 \cdot \hat{g}_2 = \langle \hat{g}_1 \hat{g}_2 \rangle = \frac{1}{r_1 r_2} \left\langle \overline{R}_1^\dagger \hat{e}_z \overline{R}_1 \overline{R}_2^\dagger \hat{e}_z \overline{R}_2 \right\rangle$$
$$= \frac{1}{r_1 r_2} \left\langle \overline{e}_z \overline{R}_1 \overline{R}_2^\dagger \hat{e}_z \overline{R}_2 \overline{R}_1^\dagger \right\rangle \tag{39}$$
$$= \frac{1}{r_1 r_2} \left\langle \hat{e}_z \overline{Q} \hat{e}_z \overline{Q}^\dagger \right\rangle = \frac{1}{r_1 r_2} \left(A^2 - B^2 - C^2 + D^2\right)$$

on using Eq. (23). In Eq. (39), the bracket denotes the scalar operator in which the product of two spinors is commutative as applied to $\overline{R}_1^\dagger$ and $\hat{e}_z \overline{R}_1 \overline{R}_2^\dagger \hat{e}_z \overline{R}_2$. In similar ways, one can obtain the remaining eight direction cosines between the two orbital frames to write

$$\begin{Bmatrix} \hat{r}_1 \\ \hat{g}_1 \times \hat{r}_1 \\ \hat{g}_1 \end{Bmatrix} = \frac{1}{r_1 r_2} \begin{bmatrix} A^2 + B^2 - C^2 - D^2 & 2(BC + AD) & 2(BD - AC) \\ 2(BC - AD) & A^2 - B^2 + C^2 - D^2 & 2(CD + AB) \\ 2(BD + AC) & 2(CD - AB) & A^2 - B^2 - C^2 + D^2 \end{bmatrix} \begin{Bmatrix} \hat{r}_2 \\ \hat{g}_2 \times \hat{r}_2 \\ \hat{g}_2 \end{Bmatrix} \tag{40}$$

which generalizes Eq. (A18). With the relation

$$\overline{Q}\,\overline{Q}^\dagger = \overline{R}_1 \overline{R}_2^\dagger \overline{R}_2 \overline{R}_1^\dagger = r_1 r_2 = A^2 + B^2 + C^2 + D^2 \tag{41}$$

Eq. (40) yields $\hat{r}_1 = \hat{r}_2$, and

$$\begin{Bmatrix} \hat{g}_1 \times \hat{r}_1 \\ \hat{g}_1 \end{Bmatrix}_\chi = \frac{1}{A^2 + B^2} \begin{bmatrix} A^2 - B^2 & 2AB \\ -2AB & A^2 - B^2 \end{bmatrix} \begin{Bmatrix} \hat{g}_2 \times \hat{r}_2 \\ \hat{g}_2 \end{Bmatrix}_\chi \tag{42}$$

at crossovers ($C = D = 0$).

With the relations

$$\dot{\hat{r}}_1 = \frac{g_1}{r_1^2} \hat{g}_1 \times \hat{r}_1, \qquad \dot{\hat{r}}_2 = \frac{g_2}{r_2^2} \hat{g}_2 \times \hat{r}_2 \tag{43}$$

Eq. (42) states that, at crossovers, the angle between $\hat{g}_1$ and $\hat{g}_2$ is same as that of $\dot{\hat{r}}_1$ and $\dot{\hat{r}}_2$. (The ground-track crossing angle is essentially formed by two osculating orbital planes instantaneously passing through the crossover point. When observed from the earth-fixed frame, the orientations of the orbital planes can be effectively represented by the unit vectors $\hat{g}_1$ and $\hat{g}_2$.) We can write

$$\cos \Lambda_\chi = \frac{A^2 - B^2}{A^2 + B^2}, \qquad \sin \Lambda_\chi = \frac{2AB}{A^2 + B^2} \tag{44}$$

so that the correct quadrant of the crossing angle Λ_χ is defined in $[0°, 360°)$.

With Eq. (44), Eq. (37) yields

$$J_\chi = \frac{1}{4} \frac{g_1}{r_1} \frac{g_2}{r_2} \sin \Lambda_\chi \tag{45}$$

Meanwhile, with Eq. (43), Eq. (16) can be written as

$$G_\chi = \left(\frac{g_1}{r_1^2} \frac{g_2}{r_2^2} \sin \Lambda_\chi \right)^2 \tag{46}$$

We therefore obtain a simple relation

$$G_\chi = \left(\frac{4 J_\chi}{r_1 r_2} \right)^2 \tag{47}$$

between the Jacobian (appearing in the spinor-version iteration scheme) and the Gaussian curvature (in the vector-version) at crossovers.

4 Number of crossovers

The ground-track crossing condition derived in the previous section is exact and general as far as the geocentric nadir mapping is concerned. Given orbital ephemerides of two satellites in their finite mission periods, the crossover locating problem is now reduced to solve the crossing condition. How many crossovers exist? And when do they (pairs of time-tags) occur? Strictly speaking, the number of solutions can be a priori unknown as highly perturbed, irregularly maneuvered satellites can generate significantly complicated ground-track patterns, and there is nothing special about any crossover point from either satellite's point of view. Let us consider instead the number of crossovers in nominal ground tracks. In practice, as most of geodetic satellites have near-circular orbits, nominal ground tracks often have topologically equivalent structure to true ground tracks. Nevertheless, no satisfactory answer has been given to the question regarding the number of crossover solutions between two nominal ground tracks (even for single-satellite nominal ground tracks as discussed before).

We first consider the single-satellite nominal ground-track crossing by representing the spinor $\overline{Q}$ in terms of Euler angles which are less useful than spinor components for numerical purposes but superior in providing some qualitative insights. Substituting Eq. (A48) into Eq. (24), with some trigonometry one can derive

$$\begin{aligned} A &= \sqrt{r_1 r_2}(-\sin\tau_- \cos i_+ \sin\vartheta_- + \cos\tau_- \cos i_- \cos\vartheta_-) \\ B &= \sqrt{r_1 r_2}(+\sin\tau_+ \sin i_+ \sin\vartheta_- + \cos\tau_+ \sin i_- \cos\vartheta_-) \\ C &= \sqrt{r_1 r_2}(+\cos\tau_+ \sin i_+ \sin\vartheta_- - \sin\tau_+ \sin i_- \cos\vartheta_-) \\ D &= \sqrt{r_1 r_2}(+\cos\tau_- \cos i_+ \sin\vartheta_- + \sin\tau_- \cos i_- \cos\vartheta_-) \end{aligned} \tag{48}$$

with

$$\begin{aligned} &\tau_\pm = \tfrac{1}{2}(\tau_1 \pm \tau_2), \quad i_\pm = \tfrac{1}{2}(i_1 \pm i_2), \\ &\vartheta_- = \tfrac{1}{2}(\vartheta_1 - \vartheta_2) \end{aligned} \tag{49}$$

From the last two equalities in Eq. (48), with $i_1 = i_2 = i$, $q_1 = q_2 = q$, $\lambda_{e_1} = \lambda_{e_2} = \lambda_e$, and $\vartheta_- = -q\tau_-$, the ground-track crossing condition $C = 0$ and $D = 0$ yield

$$\cos\tau_+ \sin q\tau_- \sin i = 0 \tag{50}$$

and

$$\cos\tau_- \sin q\tau_- \cos i = \sin\tau_- \cos q\tau_- \tag{51}$$

Meanwhile we restrict our interests to a repeat period which corresponds to the two-dimensional domain $0 \le \tau_2 < \tau_1 < 2M\pi$ ($0 < \tau_- < M\pi$, $\tau_- \le \tau_+ < 2M\pi - \tau_-$) shown in Fig. 5. Note that $\sin\tau_- \ne 0$ and $\sin q\tau_- \ne 0$ as the trivial $\tau_1 = \tau_2 (\tau_- = 0)$ is excluded, and that Eqs. (50) and (51) show the uncoupling of τ_+ and τ_-. While Eq. (50) is reduced to $\cos\tau_+ = 0$ and readily yields $2M$ solutions for $0 \le \tau_+ < 2M\pi$, Eq. (51) can be written as

$$(1 - \cos i)\sin\left[(M+N)\frac{\tau_-}{M}\right] = (1 + \cos i)\sin\left[(M-N)\frac{\tau_-}{M}\right] \tag{52}$$

since $q = N/M$.

Let L denote the number of solutions in Eq. (52) for $0 < \tau_- < M\pi$. We immediately note $L = M + N - 1$ and $L = ||M - N| - 1|$, respectively, for the limiting cases of $\cos i = -1$ and $\cos i = 1$. To investigate the variation of L in $-1 < \cos i < 1$, we decompose Eq. (51) into

$$\cos\tau_- = \cos q\tau_- = 0 \tag{53}$$

and

$$\cos i = K(\tau_-) = \frac{\sin\tau_- \cos q\tau_-}{\cos\tau_- \sin q\tau_-} \tag{54}$$

where the function K is introduced for convenience. Note that Eq. (53) yields at most one solution $\tau_- = M\pi/2$ which exists when both M and N are odd. This peculiar solution corresponds to crossovers at the equator, whereas Eq. (54) yields nonequatorial crossovers (if they exist). For an example case of $q = 5/9$, Fig. 6 presents the $(\tau_-, \cos i)$ solution loci of Eqs. (53) and (54) showing that L varies from 13 to 3 as the value

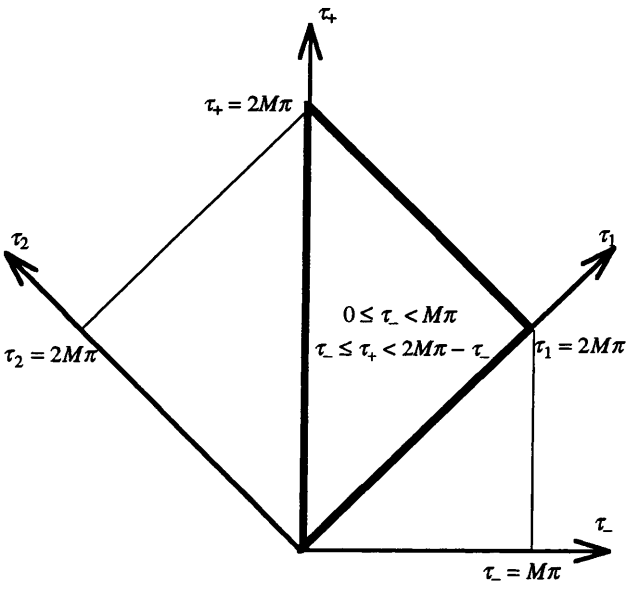

Fig. 5. The (τ_1, τ_2) domain for single-satellite nominal crossover solutions

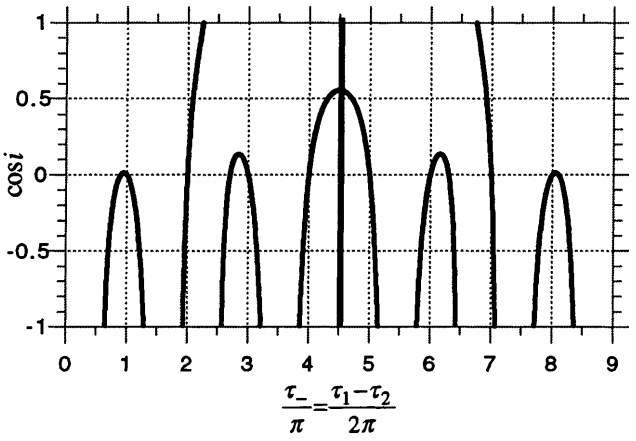

Fig. 6. Loci of single-satellite nominal crossover solutions in $(\tau_-, \cos i)$ plane for $q = 5/9$

of $\cos i$ varies from -1 to 1. Note that the changes of L occur at the five maximal points of the function K.

Now consider the differentiation of K in Eq. (54),

$$K'(\tau_-) = \frac{\sin q\tau_- \cos q\tau_- - q\sin\tau_- \cos\tau_-}{(\cos\tau_- \sin q\tau_-)^2} \tag{55}$$

where the prime indicates differentiation with respect to τ_-. Let τ_-^* be an extremal solution of K such that it satisfies $K'(\tau_-^*) = 0$, or equivalently

$$\frac{\cos q\tau_-^*}{\cos\tau_-^*} = q\frac{\sin\tau_-^*}{\sin q\tau_-^*} \tag{56}$$

on using the numerator in Eq. (55).

Let $K^* = K(\tau_-^*)$ denote an extremum of the function K. Using Eqs. (54) and (56), one can verify

$$K^* = q\left(\frac{\sin\tau_-^*}{\sin q\tau_-^*}\right)^2 = q^{-1}\left(\frac{\cos q\tau_-^*}{\cos\tau_-^*}\right)^2 \ge 0 \tag{57}$$

and

$$(K^* - q)(K^* - q^{-1}) = \left(\frac{\cos^2\tau_-^* - \cos^2 q\tau_-^*}{\cos\tau_-^* \sin q\tau_-^*}\right)^2 \ge 0 \tag{58}$$

which indicate the range of the extremun K^*. In other words, the function K is monotone when $K < 0$ and when $\min(q, q^{-1}) < K < \max(q, q^{-1})$. As shown in Fig. 6, the value of L changes at the extrema. Varying the inclination, the value of L can change only in the mixed region in the $(q, \cos i)$ space shown in Fig.1. In summary, we have

$$\begin{cases} L = M + N - 1 & \text{in } -1 \le \cos i < 0 \\ ||M - N| - 1| \le L \le M + N - 1 & \text{in } 0 < \cos i < \min(q, q^{-1}) \\ L = ||M - N| - 1| & \text{in } \min(q, q^{-1}) < \cos i \le 1 \end{cases} \tag{59}$$

which verifies the discussion presented in Sect. 2. There exist $2ML$ crossover solutions (the combination of the $2M$ solutions of τ_+ and the L solutions of τ_-) in the two-dimensional domain of $(0 < \tau_- < M\pi,\ 0 \le \tau_+ < 2M\pi)$.

Since we are working in its semidomain ($0 < \tau_- < M\pi,\ \tau_- \le \tau_+ < 2M\pi - \tau_-$), we say that the number of single-satellite nominal crossovers is ML.

As we have seen in the two-dimensional parametric space of single-satellite cases (which forms a subspace of the five-dimensional parametric space of dual-satellite cases), changes may occur in the number of crossover solutions in the mixed region $0 < \cos i < \min(q, q^{-1})$. These changes correspond to "bifurcations" (Guckenheimer and Holmes 1986, p. 117): the term originally used to describe the splitting of equilibrium solutions in a family of differential equations at parametric points or regions where the Jacobian derivative of the differential equations has a zero eigenvalue. In our case, the splitting of crossover solutions occurs where the Jacobian of the ground-track crossing condition Eq. (26) is singular. We know that the Jacobian vanishes when the ground-track crossing angle becomes 0° or 180°. In other words, as it can be quite naturally understood, births and deaths of crossover solutions can occur at parametric regions where the two ground tracks can be collinear. Such regions will be referred to as bifurcating regions.

We now return to the ground-track slope equation (5). One can write the ground-track collinear condition by

$$\left(\frac{1}{\cos\phi}\frac{\mathrm{d}\phi}{\mathrm{d}\lambda}\right)_1 = \left(\frac{1}{\cos\phi}\frac{\mathrm{d}\phi}{\mathrm{d}\lambda}\right)_2 \tag{60}$$

which yields

$$\begin{aligned}&\sqrt{\cos^2\phi - \cos^2 i_2}\left(\cos i_1 - q_1\cos^2\phi\right)\\ &= \pm\sqrt{\cos^2\phi - \cos^2 i_1}\left(\cos i_2 - q_2\cos^2\phi\right)\end{aligned} \tag{61}$$

where, in the dual sign, "plus" is for the 0° crossing angle cases (i.e., both tracks are north-going or south-going) and "minus" is for the 180° crossing angle cases (i.e., one track is north-going and the other south-going). It is noteworthy that Δ is absent in Eq. (61), and we can therefore work with a four-dimensional parametric space of (i_1, i_2, q_1, q_2) to search the bifurcating regions. As the roles of two tracks can be exchanged, we can set $q_2 \ge q_1$. Taking squares of both sides, Eq. (61) can be written as

$$\begin{aligned}&X\cos^6\phi + Y\cos^4\phi + Z\cos^2\phi = 0\\ &\quad\text{with}\quad \max\left\{\cos^2 i_1, \cos^2 i_2\right\} \le \cos^2\phi \le 1\end{aligned} \tag{62}$$

and

$$\begin{cases} X &= q_1^2 - q_2^2\\ Y &= 2(q_2\cos i_2 - q_1\cos i_1)\\ &\quad +\left(q_2^2\cos^2 i_1 - q_1^2\cos^2 i_2\right)\\ Z &= \cos^2 i_1 - \cos^2 i_2\\ &\quad +2\cos i_1\cos i_2(q_1\cos i_2 - q_2\cos i_1)\end{cases} \tag{63}$$

Equation (62) is a cubic equation in $\cos^2\phi$. Excluding the peculiar triple solution $\cos^2\phi = 0$, which can occur when both ground tracks are circumpolar, it is essentially a quadratic equation and may yield 0, 1, or 2 real solutions depending on the parametric values. The existence of a solution (or solutions) implies that the corresponding parametric point is in bifurcating regions where the number of crossovers can be changed as the parameter values vary.

In Fig. 7 we display eleven (i_1, i_2) sections of the (i_1, i_2, q_1, q_2) space by varying the values of (q_1, q_2). The eleven points (A–K) in the (q_1, q_2) section at the right lower corner depict the approximate values of (q_1, q_2) corresponding to the eleven (i_1, i_2) sections. In each of the (i_1, i_2) sections, bifurcation regions are striped (horizontally, vertically, or in both ways). The horizontally striped regions correspond to the existence of the 0° crossing angle solution, and the vertically striped regions correspond to the existence of the 180° crossing angle solution. While both roots exist in the regions where the horizontal stripes and vertical stripes cross, no real root exists in the white areas, which will be called regular regions. The lines labeled a–g are

$$\begin{aligned}&\text{a.}\ \ \sin(i_2 - i_1) = q_1\sin i_2 - q_2\sin i_1\\ &\text{b.}\ \ \sin(i_2 + i_1) = q_1\sin i_2 + q_2\sin i_1\\ &\text{c.}\ \ \cos i_1 = +\cos i_2\\ &\text{d.}\ \ \cos i_1 = -\cos i_2\\ &\text{e.}\ \ q_2\cos i_2 = 1\\ &\text{f.}\ \ q_1\cos i_1 = 1\\ &\text{g.}\ \ Y^2 - 4XZ = 0\end{aligned} \tag{64}$$

at which the characteristics of the parametric space can be significantly changed.

In each of the eleven sections, there essentially exist four regular regions (left, right, lower, and upper white areas) which are separated by the diagonal and antidiagonal bifurcating regions. We focus our discussion on the section $\mathrm{A}(q_1 = N_1/M_1 = 1/3, q_2 = N_2/M_2 = 1/2)$ which is typical for two satellites below the geosynchronous altitude (i.e., $q < 1$). In each of the four regular regions, the number of crossovers is invariant. Since one can consider the four limiting points ($i_1 = 0°$, $i_2 = 90°$), ($i_1 = 180°$, $i_2 = 90°$), ($i_1 = 90°$, $i_2 = 0°$), ($i_1 = 90°$, $i_2 = 180°$) as representative points of the four regular regions, the corresponding numbers of crossovers are readily summarized as $2M_2|M_1 - N_1|$, $2M_2(M_1 + N_1)$, $2M_1|M_2 - N_2|$, $2M_1(M_2 + N_2)$, respectively. For instance, with ($i_1 = 0°$, $i_2 = 90°$) each of the M_2 revolutions of the circumpolar ground track crosses with each of the $|M_1 - N_1|$ revolutions of the eastward equatorial track twice (one along its ascending trace and one along its descending trace). In the bifurcating regions, the number of crossovers cannot be easily guessed and may depend on the value of the remaining parameter Δ. In fact, the ground-track crossing can be highly sensitive to small changes in any of the five parameters. For actual ground tracks, such a small change can be easily introduced as the parameters experience perturbed variations.

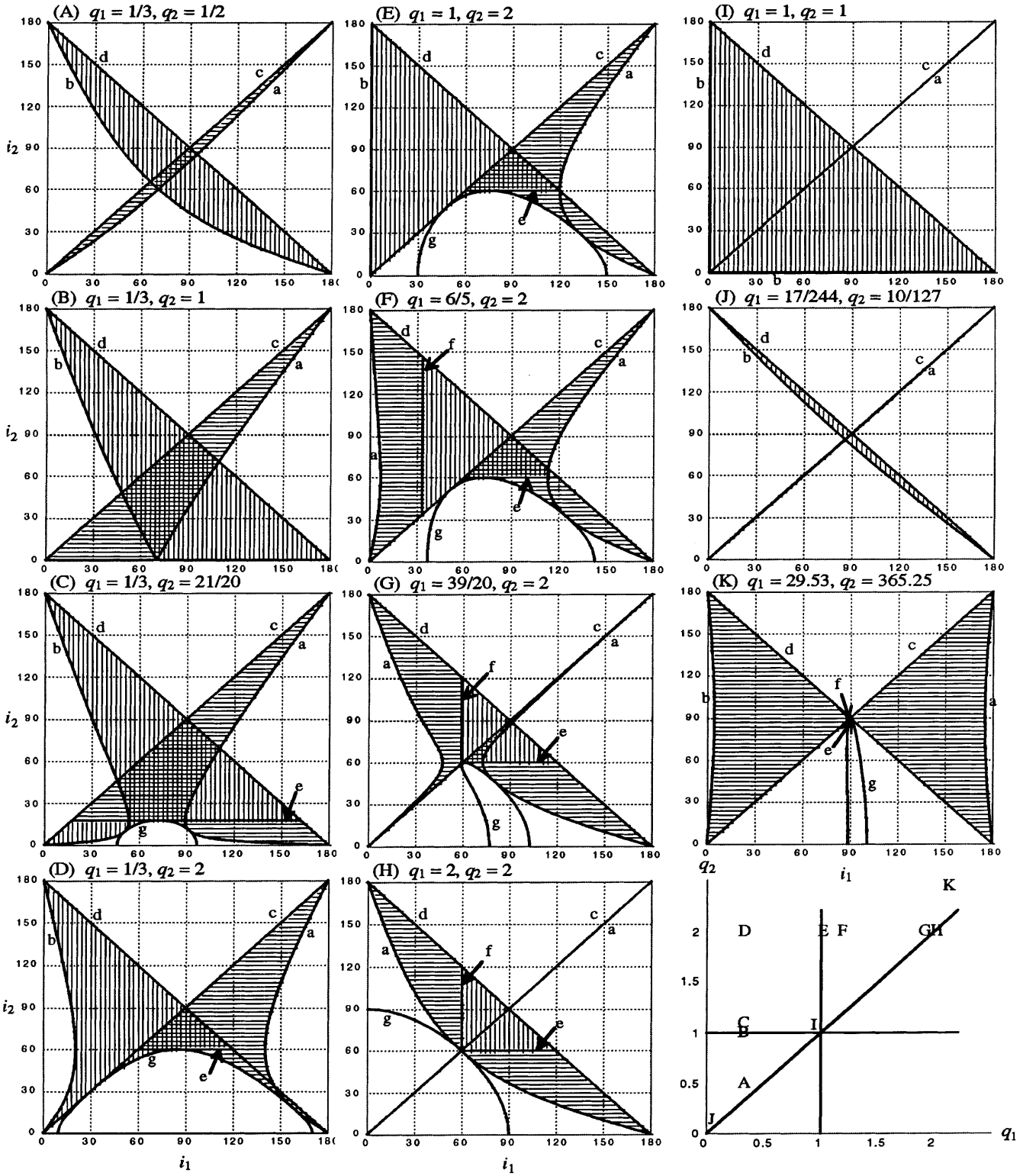

Fig. 7. Examples of (i_1, i_2) parametric sections

5 Applications

We now aim to find crossovers associated with ephemerides of actual satellites. Those satellites are GEOSAT (which flew from March 1985 to December 1989), ERS-1 (which has been orbiting since 22 April 1991), and TOPEX/POSEIDON (which has been orbiting since 10 August 1992). For each of the three satellites, after checking their repeatability using the ephemerides to be described, we selected a complete repeat cycle: 17.050458355 days from 02:55:43 10 April 1987 in the GEOSAT Exact Repeat Mission (ERM), 34.999940729

days from 03:45:56 22 February 1993 in the ERS-1 Phase-C mission, and 9.915647338 days from 04:29:45 2 March 1994 in the TOPEX/POSEIDON mission. The three repeat missions have, respectively, $(i_G \approx 108^\circ, q_G \approx N_G/M_G \approx 17/244)$, $(i_E \approx 98.5^\circ, q_E \approx N_E/M_E = 35/501)$, and $(i_T \approx 66^\circ, q_T \approx N_T/M_T \approx 10/127)$ where the subscripts denote mission initials. We can say that the GEOSAT and ERS-1 ground tracks are retrograde westward, and the TOPEX/POSEIDON ground track is posigrade eastward.

Orbital trajectories of actual satellites are often provided in terms of tabulated ephemerides. In addition to the TOPEX/POSEIDON ephemerides (Tapley et al. 1994), the GEOSAT-ERM and ERS-1 Phase-C ephemerides used were consistently generated using the UTOPIA orbit determination software system at the Center for Space Research at the University of Texas at Austin. Each of the three satellites' orbital trajectories was given in the form of a discretely tabulated time-series of earth-fixed geocentric equatorial Cartesian states at 10-s intervals. For usage of such tabulated states in the search of ground-track crossovers, we need an efficient and accurate interpolator to compute the state at any instant time in the table. For the state interpolation, we adopted the Hermite interpolation scheme (Ferziger 1981, p. 12). To find the location of a specific time in the state tables, the routine "hunt" in Press et al. (1922, pp. 111–113) is used.

The spherical earth so far used to describe ground tracks can be replaced by a more realistic earth-surface model. Let the subsatellite point $\bar{r}_o = \{x_o, y_o, z_o\}$ be a normal projection of the satellite's position $\bar{r} = \{x, y, z\}$ onto a generalized earth-surface model $E(\bar{r}_o) = 0$. The surface normal projection to minimize the satellite's altitude above the surface can be formulated by

$$\textit{Minimize } P(\bar{r}_o, \eta) = |\bar{r} - \bar{r}_o|^2 + \eta E(\bar{r}_o) \tag{65}$$

where η is the Lagrange multiplier. A proper earth-surface model is the geoid, especially for oceanographic applications of satellite altimetry, as employed by Shum (1982) by utilizing a spherical harmonics geopotential model. In practice, as it is widely adopted in satellite geodesy, the geoid is well approximated by a reference ellipsoid of revolution (Torge 1991, pp. 44–49) with its semimajor axis a_e and semiminor axis b_e, such that

$$E = x_o^2 + y_o^2 + kz_o^2 - a_e^2 \quad \text{with} \quad k = \frac{a_e^2}{b_e^2} \tag{66}$$

Albeit for the ellipsoidal nadir mapping, closed-form formulas exist with some complexities (Grafarend and Lohse 1991), we prefer the sequences

$$x_o = \frac{x}{1+\eta}, \;\; y_o = \frac{y}{1+\eta}, \;\; z_o = \frac{z}{1+k\eta}$$

$$E = x_o x_o + y_o y_o + k z_o z_o - a_e^2$$

$$x_o^\eta = \frac{-x_o}{1+\eta}, \;\; y_o^\eta = \frac{-y_o}{1+\eta}, \;\; z_o^\eta = \frac{-kz_o}{1+k\eta}$$

$$E^\eta = 2\left(x_o x_o^\eta + y_o y_o^\eta + k z_o z_o^\eta\right)$$

$$\eta \leftarrow \eta - \frac{E}{E^\eta}$$

Iterate if $|E|$ isn't small enough

$$x_o^t = \frac{\dot{x}}{1+\eta}, \;\; y_o^t = \frac{\dot{y}}{1+\eta}, \;\; z_o^t = \frac{\dot{z}}{1+k\eta}$$

$$E^t = 2\left(x_o x_o^t + y_o y_o^t + k z_o z_o^t\right)$$

$$\dot{\eta} = -\frac{E^t}{E^\eta}$$

$$\dot{x}_o = x_o^t + \dot{\eta} x_o^\eta, \;\; \dot{y}_o = y_o^t + \dot{\eta} y_o^\eta, \;\; \dot{z}_o = z_o^t + \dot{\eta} z_o^\eta$$

starting from a proper positive value of η. The superscript t and η appearing in the above equations imply partial differentiations. Although the ground-track crossing condition derived before was based on the mapping of satellite states to a spherical-earth model, it is noteworthy that a generalized surface mapping can be reflected simply by using the nadir-mapped ground-track states instead of the satellite's orbital states in constructing the crossing condition and solving it to find crossovers. Here, for the computation of the three satellites' ground tracks, we use the ellipsoidal nadir mapping of satellite states on the TOPEX/POSEIDON standard reference ellipsoid of revolution with $a_e = 6378136.3\,\text{m}$ and $b_e = 6356751.6\,\text{m}$ (the reciprocal flattening of 298.257).

To find actual crossovers, one can pursue an approach specific to a particular combination of ground tracks. However, in general we have to map out the full (t_1, t_2) domain. "There are no good, general methods for solving systems of more than one nonlinear equation" as stated in Press et al. (1992, p. 372). Here, we pursue a grid-search scheme by setting initial guesses of solutions on a regular grid of the corresponding (t_1, t_2) domain; the grid scheme can be outlined as

Loop for $(t_{1k} = t_{1i};\ t_{1k} \le t_{1f};\ t_{1k} = t_{1k} + \Delta t_1)$
  Loop for $(t_{2k} = t_{2i};\ t_{2k} \le t_{2f};\ t_{2k} = t_{2k} + \Delta t_2)$
    0. Initialize iteration: $\{t_1, t_2\} = \{t_{1k}, t_{2k}\}$;
    1. Compute $a_1, b_1, c_1, d_1, \dot{a}_1, \dot{b}_1, \dot{c}_1, \dot{d}_1$ at t_1 and $a_2, b_2, c_2, d_2, \dot{a}_2, \dot{b}_2, \dot{c}_2, \dot{d}_2$ at t_2;
    2. Compute $C_{t_1}, D_{t_1}, C_{t_2}, D_{t_2}$ using Eq. (28);
    3. Compute J using Eq. (29);
    4. If J is tiny, abort iteration;
    5. Update $\{t_1, t_2\}$ using Eq. (27);
    6. If $|t_1 - t_{1k}| > p\Delta t_1$ or $|t_2 - t_{2k}| > p\Delta t_2$, abort iteration;
    7. Compute C, D using Eq. (24);
    8. If C and D are not sufficiently small, go to 1;
    9. If $t_{1i} \le t_1 \le t_{1f}$ and $t_{2i} \le t_2 \le t_{2f}$, store $\{t_1, t_2\}$ as a crossover time-tag pair;
  End Loop
End Loop

Sort the stored crossover time-tag pairs and remove duplicated pairs.

In this outline, t_{1i} and t_{1f} denote the initial and final times for the first satellite, t_{2i} and t_{2f} denote the initial and final times for the second satellite, t_{1k} and t_{2k} denote

initial guesses of crossover solutions on the grid knots, Δt_1 and Δt_2 denote the grid-knot steps, and p denotes a parameter to determine the extent of duplicated survey by controlling the size of a box, which is centered at the initial grid knot $\{t_{1k}, t_{2k}\}$ and brackets the solution search. For the computation of spinor states, we need interpolation of the vector states using ephemerides tables, their nadir mappings, and vector-to-spinor ground-track state transformations. The outline is written for an illustrative purpose of a general dual-satellite crossover locating problem, and may not be an optimal scheme for a specific problem.

There are six ground-track configurations for the three repeat cycles of GEOSAT-ERM, ERS-1, and TOPEX/POSEIDON; three single-satellite cases and three dual-satellite cases. With the Hermite state interpolator, the ellipsoidal nadir mapping, and the two-way transformations between the vector and spinor states at our disposal, we applied the grid-search scheme to all the six cases. We have deployed the initial guesses of crossover solutions on a $1/8 \times 1/8$-revolution grid regardless of single- or dual-satellite ground-track scenarios. In other words, the grid-knot step size is 754.69, 754.49, and 843.22 s, respectively for GEOSAT-ERM, ERS-1, and TOPEX/POSEIDON. We used $p = 1.0$ so that the search at a grid knot covers a $1/4 \times 1/4$-revolution box.

The number of single-satellite crossovers numerically found are 63440, 268035, and 14732, respectively for the three cycles. These numbers agree exactly with the number of nominal single-satellite crossovers $M_G(M_G + N_G - 1)$, $M_E(M_E + N_E - 1)$, $M_T(M_T - N_T - 1)$ of the three repeat missions. The number of dual-satellite crossovers found are 261522, 117234, 57638, respectively, for the three combinations of GEOSAT-ERM and ERS-1, ERS-1 and TOPEX/POSEIDON, and GEOSAT-ERM and TOPEX/POSEIDON. The first two numbers exactly match with $2M_E(M_G + N_G)$ and $2M_E(M_T - N_T)$, indicating that they are located at the regular regions. However the number of crossovers between the GEOSAT-ERM and TOPEX/POSEIDON cannot be easily explained. Returning to Fig. 7 and seeing the section $J(q_1 = 17/244,\ q_2 = 10/127)$, which is topologically equivalent to the section A, one may approximately locate the parametric point $(i_1 \approx 108^\circ,\ i_2 \approx 66^\circ)$ corresponding to the dual ground tracks of the GEOSAT-ERM and TOPEX/POSEIDON. The point is located in the vertically striped bifurcating region along the diagonal. It is located between the lower regular region and the right regular region and the number 57638 is between $2M_G(M_T - N_T) = 57096$ and $2M_T(M_G + N_G) = 66294$. For the combination of the GEOSAT-ERM and TOPEX/POSEIDON, Eq. (62) yields a real solution $\cos^2 \phi = 0.785$, indicating that crossovers near 27.5°S or 27.5°N have small acute angle and therefore a slight perturbation can easily generate or destroy crossovers. These results support the bifurcation analysis presented in the previous section.

6 Conclusions

Techniques to locate satellite ground-track crossovers have been frequently presented as an auxiliary procedure of other main topics related to the applications of satellite altimetry. In this paper, we have studied the issue as an independent topic. The principal new aspects investigated (or presented) herein are: (1) classification of idealized nominal ground tracks in the two-dimensional parametric space of $(q, \cos i)$ (2) classification of dual-satellite nominal ground-track bifurcations in the four-dimensional parametric space of (i_1, i_2, q_1, q_2) in conjunction with the number of crossover solutions, and (3) numerical searching schemes of actual crossovers in both vector and spinor forms. Indeed, some of these interesting aspects seem not to have been surveyed before.

In a problem related to satellite orbits, a proper selection of variables often leads to simplification of the problem, as we have used the spinor representation of the satellite state to establish the ground-track crossing condition. In satellite altimetry, a more conventional crossover locating method is based on usage of the geodetic latitude and longitude, see, e.g., Rowlands (1981) or Wisse et al. (1995, pp. 72–76). The use of geodetic coordinates originated from the fact that the satellite-altimeter geophysical data record (GDR) already contains them along with the altimeter-range measurement, its time-tag, and other environmental/geophysical corrections. However, when one pursues the direct locating of crossovers from satellite-state tables, the vectors or spinors will be more adequate. Once the unknown crossover time-tags are obtained, it is a matter of data hunting and interpolation to get the corresponding altimeter data records. One may also prefer the vector version of the iteration scheme to the spinor version, as it can be more understandable. The main advantage of using spinors is that a converged solution of iteration always yields a crossover. The main disadvantage of using spinors is that, as the satellite states are usually given by Cartesian vectors, one needs conversions between the vector and spinor state. There is a trade-off unless the satellite states are initially given by spinors. However, since no trigonometrics are involved in the state conversions, the increase of computational labor produced by using the spinor- language should not be overestimated. The selection of variables will be highly dependent on one's object.

Acknowledgements. Thanks are due to B. Tapley, B. Schutz, and R. Eanes for their encouragement and interest on this subject, to J. Ries for providing ephemerides of the three altimeter satellites, to S. Bettadpur for reading a part of the paper in its first draft, and to Y. Hahn in Jet Propulsion Laboratory and M. Anzenhofer in GFZ (GeoForschungsZentum, Potsdam) for finding some references. Sincere appreciation is due to anonymous reviewers whose comments were helpful in improving the paper.

Appendix

Satellite state in spinor space

Let $\{\hat{e}_x, \hat{e}_y, \hat{e}_z\}$ and $\{\hat{e}_u, \hat{e}_v, \hat{e}_w\}$ be right-handed orthogonal triads of geocentric unit vectors which form the rotating earth-fixed frame and the non- rotating inertial frame, respectively. In the spinor algebra, which forms a subalgebra of the so-called Clifford algebra [geometric algebra in Hestenes (1983)], such a triad corresponds to the Pauli spin matrices (Goldstein 1980, p.156) and yields the spinor multiplication laws (Cartan 1981, p.44; Landau and Lifshitz 1977, p.202), e.g.,

$$\begin{aligned} &\hat{e}_x\hat{e}_x = \hat{e}_y\hat{e}_y = \hat{e}_z\hat{e}_z = 1 \\ &\hat{e}_x\hat{e}_y = j\hat{e}_z = -\hat{e}_y\hat{e}_x \text{ (in cyclic order)} \end{aligned} \tag{A1}$$

where j is the unit imaginary number.

Let $\bar{v}_1 = b_1\hat{e}_x + c_1\hat{e}_y + d_1\hat{e}_z$ and $\bar{v}_2 = b_2\hat{e}_x + c_2\hat{e}_y + d_2\hat{e}_z$ be two arbitrary vectors. With the multiplication laws of Eq. (A1), one can readily verify the relation

$$\overline{v}_1\overline{v}_2 = \overline{v}_1 \cdot \overline{v}_2 + j\,\overline{v}_1 \times \overline{v}_2 \tag{A2}$$

between the spinor product, the scalar product, and the vector product of the two vectors. Equation (A2) can be also represented by

$$\begin{aligned} &\overline{v}_1 \cdot \overline{v}_2 = \tfrac{1}{2}(\overline{v}_1\overline{v}_2 + \overline{v}_2\overline{v}_1) \\ &\overline{v}_1 \times \overline{v}_2 = -\tfrac{1}{2}j(\overline{v}_1\overline{v}_2 - \overline{v}_2\overline{v}_1) \end{aligned} \tag{A3}$$

The spinor space is a combination of the scalar and vector spaces such that a spinor $\overline{R} = a + j\,\overline{v}$ and its conjugate $\overline{R}^\dagger = a - j\,\overline{v}$, where $\overline{v} = b\hat{e}_x + c\hat{e}_y + d\hat{e}_z$, are defined by the four real-valued scalar components $\{a, b, c, d\}$. It is equivalent to the two-dimensional complex vector space appearing in quantum mechanics in conjunction with the wave functions (Greiner 1994, p. 306). We will frequently denote the scalar part of $\overline{R}$ with $\langle\overline{R}\rangle$, i.e.,

$$\langle\overline{R}\rangle = a = \langle\overline{R}^\dagger\rangle = \tfrac{1}{2}(\overline{R} + \overline{R}^\dagger) \tag{A4}$$

where the bracket $\langle\ \rangle$ will be called the scalar operator.

Let $\overline{R}_1 = a_1 + j\,\overline{v}_1$ and $\overline{R}_2 = a_2 + j\,\overline{v}_2$ be two arbitrary spinors. With Eq. (A2), one obtains

$$\begin{aligned} \overline{R}_1\overline{R}_2^\dagger &= (a_1 + j\,\overline{v}_1)(a_2 - j\,\overline{v}_2) \\ &= a_1a_2 + \overline{v}_1 \cdot \overline{v}_2 + j(a_2\overline{v}_1 - a_1\overline{v}_2 + \overline{v}_1 \times \overline{v}_2) \end{aligned} \tag{A5}$$

which can be further expanded in terms of the real components $\{a_1, b_1, c_1, d_1\}$ and $\{a_2, b_2, c_2, d_2\}$ to yield the equations given in Eq. (24) in the main text.

The products of the two spinors are in general not commutative, e.g., $\overline{R}_1\overline{R}_2^\dagger \neq \overline{R}_2^\dagger\overline{R}_1$. But they are commutative inside the scalar operator, i.e., with Eq. (A5), we have

$$\begin{aligned} \langle\overline{R}_1\overline{R}_2^\dagger\rangle &= \langle\overline{R}_2^\dagger\overline{R}_1\rangle = a_1a_2 + \overline{v}_1 \cdot \overline{v}_2 \\ &= a_1a_2 + b_1b_2 + c_1c_2 + d_1d_2 \end{aligned} \tag{A6}$$

For the norm of the spinor $\overline{R}$, we use a positive scalar

$$|\overline{R}| = (\overline{R}\,\overline{R}^\dagger)^{1/2} = (\overline{R}^\dagger\overline{R})^{1/2} = (a^2 + b^2 + c^2 + d^2)^{1/2} \tag{A7}$$

The spinor $\overline{R}$ can be decomposed into $|\overline{R}|\hat{R}$ where $\hat{R}$ is a unimodular spinor (i.e., $|\hat{R}| = 1$).

The spinor algebra is equivalent to the quaternion algebra, which has long been known as the ideal tool to describe rotational motions of rigid bodies. In practice, the four components of a unimodular spinor correspond to the Euler parameters (Goldstein 1980, p. 155). For instance, the earth's rigid body rotation can be effectively represented by

$$\begin{Bmatrix} \hat{e}_x \\ \hat{e}_y \\ \hat{e}_z \end{Bmatrix} = \hat{E}^\dagger \begin{Bmatrix} \hat{e}_u \\ \hat{e}_v \\ \hat{e}_w \end{Bmatrix} \hat{E} = \overline{\omega}_e \times \begin{Bmatrix} \hat{e}_u \\ \hat{e}_v \\ \hat{e}_w \end{Bmatrix} \tag{A8}$$

where $\hat{E}$ is a unimodular spinor which accounts for the precession, nutation, spin axis rotation and polar motion of the earth (Lambeck 1988), and $\overline{\omega}_e$ is the corresponding angular velocity vector.

There is a complete analogy between the orbital angular motion of a satellite and the rotational motion of a rigid body. Let $\overline{s} = u\hat{e}_u + v\hat{e}_v + w\hat{e}_w$ represent the orbital position vector of a satellite in the geocentric inertial frame. Let $\overline{S} = \alpha + j(\beta\hat{e}_u + \gamma\hat{e}_v + \delta\hat{e}_w)$ be a spinor based on the triad $\{\hat{e}_u, \hat{e}_v, \hat{e}_w\}$. As it can be directly verified using the multiplication laws of Eq. (A1), which is also applicable to $\{\hat{e}_u, \hat{e}_v, \hat{e}_w\}$, the spinor algebra enables us to write

$$\overline{s} = \overline{S}^\dagger\hat{e}_u\overline{S} \tag{A9}$$

with

$$u = \alpha^2 + \beta^2 - \gamma^2 - \delta^2,\ \ v = 2(\beta\gamma + \alpha\delta),\ \ w = 2(\beta\delta - \alpha\gamma) \tag{A10}$$

Let s be the magnitude of $\overline{s}$. We also have

$$\begin{aligned} s = |\overline{s}| &= \left(u^2 + v^2 + w^2\right)^{1/2} = |\overline{S}|^2 = \overline{S}\,\overline{S}^\dagger = \overline{S}^\dagger\,\overline{S} \\ &= \alpha^2 + \beta^2 + \gamma^2 + \delta^2 \end{aligned} \tag{A11}$$

On differentiating Eq. (A9), we have

$$\dot{\overline{s}} = \dot{\overline{S}}^\dagger\hat{e}_u\overline{S} + \overline{S}^\dagger\hat{e}_u\dot{\overline{S}} \tag{A12}$$

which can be expanded to relate the scalar components of $\dot{\overline{s}} = \dot{u}\hat{e}_u + \dot{v}\hat{e}_v + \dot{w}\hat{e}_w$ and those of $\dot{\overline{S}} = \dot{\alpha} + j(\dot{\beta}\hat{e}_u + \dot{\gamma}\hat{e}_v + \dot{\delta}\hat{e}_w)$. One can actually write

$$\begin{bmatrix} u & \dot{u} \\ v & \dot{v} \\ w & \dot{w} \\ s & \dot{s} \end{bmatrix} = \begin{bmatrix} \alpha & \beta & -\gamma & -\delta \\ \delta & \gamma & \beta & \alpha \\ -\gamma & \delta & -\alpha & \beta \\ \alpha & \beta & \gamma & \delta \end{bmatrix} \begin{bmatrix} \alpha & 2\dot{\alpha} \\ \beta & 2\dot{\beta} \\ \gamma & 2\dot{\gamma} \\ \delta & 2\dot{\delta} \end{bmatrix} \tag{A13}$$

on using the equations in (A10), (A11), and their differentiations. As the six components of $\overline{s}$ and $\dot{\overline{s}}$ constitute the orbital state in the vector space, the eight components of $\overline{S}$ and $\dot{\overline{S}}$ constitute the orbital state in the spinor space. While Eq. (A13) stands for the spinor-to-

vector state transformation, we need more information to write its inverse transformation (note that s and $\dot{s}$ are auxiliaries and the 4×4 matrix is inherently singular).

As the vector $\overline{s}$ can be decomposed into its dilation s and rotation $\hat{s}$, i.e., $\overline{s} = s\hat{s}$, where $\hat{s}$ is the unit vector pointing $\overline{s}$, the spinor $\overline{S}$ can be also decomposed into its dilation $|\overline{S}|$ and rotation $\hat{S}$, i.e., $\overline{S} = |\overline{S}|\hat{S}$. As shown in Hestenes (1983), the unimodular spinor $\hat{S}$ can be decomposed into the Eulerian rotations, i.e.,

$$\hat{S} = \exp(j\hat{e}_w \tfrac{1}{2}\tau)\exp(j\hat{e}_u \tfrac{1}{2}i)\exp(j\hat{e}_w \tfrac{1}{2}\Omega) \tag{A14}$$

where the three Euler angles Ω, i, τ (Goldstein 1980, p. 146) correspond, respectively, to the longitude of the ascending node measured from the equinox, the inclination, and the argument of latitude of the orbit. With the relation $|\overline{S}| = s^{1/2}$, we can write

$$\overline{S} = s^{1/2}(\cos\tfrac{1}{2}\tau + j\hat{e}_w \sin\tfrac{1}{2}\tau)(\cos\tfrac{1}{2}i + j\hat{e}_u \sin\tfrac{1}{2}i) \times (\cos\tfrac{1}{2}\Omega + j\hat{e}_w \sin\tfrac{1}{2}\Omega) \tag{A15}$$

which can be expanded to yield the spinor components

$$\begin{aligned} \alpha &= s^{1/2}\cos\tfrac{1}{2}(\Omega+\tau)\cos\tfrac{1}{2}i, \quad \beta = s^{1/2}\cos\tfrac{1}{2}(\Omega-\tau)\sin\tfrac{1}{2}i \\ \gamma &= s^{1/2}\sin\tfrac{1}{2}(\Omega-\tau)\sin\tfrac{1}{2}i, \quad \delta = s^{1/2}\sin\tfrac{1}{2}(\Omega+\tau)\cos\tfrac{1}{2}i \end{aligned} \tag{A16}$$

showing their correspondence to the Euler parameters (Goldstein 1980, p. 155) and to the Cayley-Klein parameters (Whittaker 1937, p. 12).

Let $\overline{h}$ be the orbital angular momentum vector of the satellite, i.e.,

$$\overline{h} = h\hat{h} = \overline{s} \times \dot{\overline{s}} = s\hat{s} \times (\dot{s}\hat{s} + s\dot{\hat{s}}) = s^2\hat{s} \times \dot{\hat{s}} \tag{A17}$$

where the scalar h and the unit vector $\hat{h}$ represent the magnitude and direction of $\overline{h}$, respectively. Now we introduce a new triad $\{\hat{s}, \hat{h} \times \hat{s}, \hat{h}\}$, which consists of the radial, transversal, and normal unit vectors of the rotating satellite-fixed orbital frame. The spinor algebra enables us to write the transformation

$$\begin{Bmatrix} \hat{s} \\ \hat{h} \times \hat{s} \\ \hat{h} \end{Bmatrix} = \frac{1}{s}\hat{S}^{\dagger} \begin{Bmatrix} \hat{e}_u \\ \hat{e}_v \\ \hat{e}_w \end{Bmatrix} \hat{S} = \frac{1}{s} \begin{bmatrix} \alpha^2+\beta^2-\gamma^2-\delta^2 & 2(\beta\gamma+\alpha\delta) & 2(\beta\delta-\alpha\gamma) \\ 2(\beta\gamma-\alpha\delta) & \alpha^2-\beta^2+\gamma^2-\delta^2 & 2(\gamma\delta+\alpha\beta) \\ 2(\beta\delta+\alpha\gamma) & 2(\gamma\delta-\alpha\beta) & \alpha^2-\beta^2-\gamma^2+\delta^2 \end{bmatrix} \begin{Bmatrix} \hat{e}_u \\ \hat{e}_v \\ \hat{e}_w \end{Bmatrix} \tag{A18}$$

where the four-parametric representation of the 3×3 transformation matrix can be also found in classical dynamics textbooks, e.g., Goldstein (1980, p. 153). We denote the nine elements of the transformation matrix by $T_{11}, T_{12}, \ldots, T_{33}$. These can be easily obtained from the vector state $\{\overline{s}, \dot{\overline{s}}\}$, as they correspond to the Cartesian components of $\overline{s}$, $\hat{h} \times \overline{s}$, $s\hat{h}$. Note that the transverse unit vector $\hat{h} \times \hat{s}$ is pointing towards the velocity of the radial unit vector

$$\dot{\hat{s}} = \frac{h}{s^2}\hat{h} \times \hat{s} \tag{A19}$$

which itself is not a unit vector. We have

$$|\dot{\hat{s}}| = \frac{h}{s^2} \tag{A20}$$

Based on Shepperd (1978), an efficient means of computing the four components of $\overline{S}$ from the transformation matrix is to write

$$\begin{cases} 4\alpha^2 = 2T - T + s \\ 4\beta^2 = 2T_{11} - T + s \\ 4\gamma^2 = 2T_{22} - T + s \\ 4\delta^2 = 2T_{33} - T + s \end{cases} \quad \text{and} \quad \begin{cases} 4\alpha\delta = T_{12} - T_{21}, & 4\beta\gamma = T_{12} + T_{21} \\ 4\alpha\beta = T_{23} - T_{32}, & 4\gamma\delta = T_{23} + T_{32} \\ 4\alpha\gamma = T_{31} - T_{13}, & 4\beta\delta = T_{31} + T_{13} \end{cases} \tag{A21}$$

with $T = T_{11} + T_{22} + T_{33}$: the trace of the transformation matrix. Several ways exist to obtain the four unknowns, e.g.,

$$\begin{aligned} \alpha &= \pm\sqrt{\frac{T+s}{4}}, \quad \beta = \frac{T_{23} - T_{32}}{4\alpha} \\ \gamma &= \frac{T_{31} - T_{13}}{4\alpha}, \quad \delta = \frac{T_{12} - T_{21}}{4\alpha} \end{aligned} \tag{A22}$$

where the sign of α cannot be determined but can be selected freely assuming that we are working with a one-to-one correspondence, or isomorphism, between $\overline{s}$ and the pair $\pm\overline{S}$. One may say that $\overline{S}$ is a double-valued function of the transformation matrix. While the solution given in Eq. (A22) is singular when $\alpha = 0$, we can write three more solutions by changing the component to be used as the divisor. At least one nonzero component exists as long as $s \neq 0$. For numerical purposes, the optimal choice among the four possibilities corresponds to the largest among absolute values of $\alpha, \beta, \gamma, \delta$, whose magnitude order is same as that of $T, T_{11}, T_{22}, T_{33}$.

Now, to obtain the components of the time derivative $\dot{\overline{S}}$, we consider the Eulerian angular velocity vector of the orbit expressed as (Hestenes 1983)

$$\overline{\omega}_s = \frac{\mathrm{d}\tau}{\mathrm{d}t}\hat{h} + \frac{\mathrm{d}i}{\mathrm{d}t}\hat{f} + \frac{\mathrm{d}\Omega}{\mathrm{d}t}\hat{e}_w \tag{A23}$$

with

$$\hat{h} = \sin i \sin\Omega\, \hat{e}_u - \sin i \cos\Omega\, \hat{e}_v + \cos i\, \hat{e}_w \tag{A24}$$

and

$$\hat{f} = \cos\Omega\, \hat{e}_u + \sin\Omega\, \hat{e}_v \tag{A25}$$

where $\hat{f}$ represents the unit vector toward the ascending orbital node. For the time derivatives of the Euler angles, we have the Gauss variation of parameter equations (Battin 1987, p.488)

$$\frac{\mathrm{d}\Omega}{\mathrm{d}t} = \ddot{n}\frac{s}{h}\frac{\sin\tau}{\sin i}, \frac{\mathrm{d}i}{\mathrm{d}t} = \ddot{n}\frac{s}{h}\cos\tau, \frac{\mathrm{d}\tau}{\mathrm{d}t} = \frac{h}{s^2} - \ddot{n}\frac{s}{h}\frac{\sin\tau\cos i}{\sin i} \tag{A26}$$

where $\ddot{n}$ represents the normal component of the satellite acceleration.

Substituting Eqs. (A24–A26) into Eq.(23), with some manipulation, one can obtain

$$\overline{\omega}_s = \frac{1}{s}\overline{S}^{\dagger}\left(\frac{h}{s^2}\hat{e}_w + \ddot{n}\frac{s}{h}\hat{e}_u\right)S \tag{A27}$$

or

$$\overline{\omega}_s = \frac{\overline{h}}{s^2} + \ddot{n}\frac{\overline{s}}{h} \tag{A28}$$

on using the first equality in Eq. (A18). Meanwhile, the velocity vector $\dot{\overline{s}}$ can be decomposed into (Hestenes and Lounesto 1983)

$$\dot{\overline{s}} = \dot{s}\hat{s} + \overline{\omega}_s \times \overline{s} = \frac{\dot{s}}{s}\overline{s} - \tfrac{1}{2}j(\overline{\omega}_s\overline{s} - \overline{s}\,\overline{\omega}_s) = \tfrac{1}{2}(\overline{W}^{\dagger}\overline{s} + \overline{s}\overline{W}) \tag{A29}$$

with

$$\overline{W} = \frac{\dot{s}}{s} + j\,\overline{\omega}_s \tag{A30}$$

Comparing Eqs. (A12) and (A29), we obtain the time derivative,

$$\dot{\overline{S}} = \tfrac{1}{2}\overline{S}\,\overline{W} \tag{A31}$$

which can be also written as

$$\dot{\overline{S}} = \tfrac{1}{2}\overline{G}\,\overline{S} \tag{A32}$$

with

$$\overline{G} = \frac{1}{s}\overline{S}\,\overline{W}\,\overline{S}^{\dagger} = \frac{\dot{s}}{s} + j\left(\frac{h}{s^2}\hat{e}_w + \ddot{n}\frac{s}{h}\hat{e}_u\right) \tag{A33}$$

on using Eqs. (A27) and (A30). Now, with Eq. (A33), one can expand Eq. (A32) to yield the four components of $\dot{\overline{S}}$,

$$\begin{aligned} \dot{\alpha} &= \tfrac{1}{2}\left(\tfrac{\dot{s}}{s}\alpha - \tfrac{h}{s^2}\delta - \ddot{n}\tfrac{s}{h}\beta\right), \quad \dot{\beta} = \tfrac{1}{2}\left(\tfrac{\dot{s}}{s}\beta + \tfrac{h}{s^2}\gamma + \ddot{n}\tfrac{s}{h}\alpha\right) \\ \dot{\gamma} &= \tfrac{1}{2}\left(\tfrac{\dot{s}}{s}\gamma - \tfrac{h}{s^2}\beta + \ddot{n}\tfrac{s}{h}\delta\right), \quad \dot{\delta} = \tfrac{1}{2}\left(\tfrac{\dot{s}}{s}\delta + \tfrac{h}{s^2}\alpha - \ddot{n}\tfrac{s}{h}\gamma\right) \end{aligned} \tag{A34}$$

To obtain the right-hand sides in Eq. (A34) we need to know $\ddot{n}$. However, having the same instantaneous position and velocity as the true orbit, we can set $\ddot{n} = 0$, which relates the spinor state to the osculating Keplerian orbit. From Eq. (A34) one can extract

$$\gamma\dot{\alpha} + \delta\dot{\beta} - \alpha\dot{\gamma} - \beta\dot{\delta} = 0 \tag{A35}$$

and

$$-\beta\dot{\alpha} + \alpha\dot{\beta} + \delta\dot{\gamma} - \gamma\dot{\delta} = \ddot{n}\frac{s^2}{h} \tag{A36}$$

The relation in Eq. (A35) is called the spinor gauge condition (Hestenes and Lounesto 1983) and also appears in the Kustaanheimo-Stiefel transformation (Stiefel and Scheifele 1971; Deprit et al. 1994). The two relations of Eqs. (A35) and (A36) compensate the two redundancies in the spinor state.

So far we have established the two-way transformation between the vector and spinor states observed in the inertial frame. The transformation is general and equivalently applicable to states for the earth-fixed frame. To clarify, let us first denote the orbital position and velocity vectors of a satellite observed in the earth-fixed frame by $\overline{r} = x\hat{e}_x + y\hat{e}_y + z\hat{e}_z = \overline{R}^{\dagger}\hat{e}_x\overline{R}$ and $\dot{\overline{r}} = \dot{x}\hat{e}_x + \dot{y}\hat{e}_y + \dot{z}\hat{e}_z = \overline{R}^{\dagger}\hat{e}_x\overline{R} + \overline{R}^{\dagger}\hat{e}_x\dot{\overline{R}}$, where $\overline{R} = a + j(b\hat{e}_x + c\hat{e}_y + d\hat{e}_z)$ is a spinor based on the rotating earth-fixed triad $\{\hat{e}_x, \hat{e}_y, \hat{e}_z\}$. Note that $\overline{r} = \overline{s}$ but their Cartesian components are different, i.e., $\{x, y, z\} \neq \{u, v, w\}$, as they are referenced to the earth-fixed frame and the inertial frame, respectively. Also note that $\dot{\overline{r}} \neq \dot{\overline{s}}$ as the time derivatives are observed in the two different reference frames. The difference is the effects of the earth rotation, i.e.,

$$\dot{\overline{r}} = \dot{\overline{s}} - \overline{\omega}_e \times \overline{s} \tag{A37}$$

The total angular velocity (to be denoted by $\overline{\omega}_r$) of the orbit observed in the earth-fixed frame combines the orbital angular velocity and the earth-rotation effect in the sense of taking their difference, i.e.,

$$\overline{\omega}_r = \overline{\omega}_s - \overline{\omega}_e \tag{A38}$$

and therefore the total angular momentum $\overline{g} = \overline{r} \times \dot{\overline{r}}$ is due to the orbital angular momentum $\overline{h} = \overline{s} \times \dot{\overline{s}}$ and the earth-rotation effect, i.e.,

$$\overline{g} = \overline{h} - \overline{r} \times \overline{\omega}_e \times \overline{r} = \overline{h} - r^2\overline{\omega}_e + (\overline{r} \cdot \overline{\omega}_e)\overline{r} \tag{A39}$$

on using Eq. (A37).

Substituting Eq. (A28) into Eq. (A38) and using Eq. (A39), we can write

$$\overline{\omega}_r = \frac{\overline{g}}{r^2} + \ddot{m}\frac{\overline{r}}{g} \tag{A40}$$

with

$$\ddot{m}\frac{r}{g} = \ddot{n}\frac{s}{h} - \hat{r}\cdot\overline{\omega}_e \tag{A41}$$

where $\ddot{m}$ can be called the normal component acceleration of the satellite effective in the rotating earth-fixed frame.

Note that the two two-way transformations $(u,v,w,\dot{u},\dot{v},\dot{w}) \leftrightarrow (\alpha,\beta,\gamma,\delta,\dot{\alpha},\dot{\beta},\dot{\gamma},\dot{\delta})$ and $(x,y,z,\dot{x},\dot{y},\dot{z}) \leftrightarrow (a,b,c,d,\dot{a},\dot{b},\dot{c},\dot{d})$ are equivalent under Eq. (A41) which is nothing but $\hat{r}\cdot\overline{\omega}_r = \hat{r}\cdot\overline{\omega}_s - \hat{r}\cdot\overline{\omega}_e$. We can write the counterparts of Eqs. (A30)–(A36) simply by using new variables. Let

$$\overline{V} = \frac{\dot{\overline{r}}}{r} + j\,\overline{\omega}_r \tag{A42}$$

then,

$$\dot{\overline{R}} = \tfrac{1}{2}\overline{R}\,\overline{V} \tag{A43}$$

and

$$\dot{\overline{R}} = \tfrac{1}{2}\overline{F}\,\overline{R} \tag{A44}$$

with

$$\overline{F} = \frac{1}{r}\overline{R}\,\overline{V}\,\overline{R}^{\dagger} = \frac{\dot{r}}{r} + j\left(\frac{g}{r^2}\hat{e}_z + \ddot{m}\frac{r}{g}\hat{e}_x\right) \tag{A45}$$

and so on.

The vector state $\{\overline{r},\dot{\overline{r}}\}$ is independent of the effective normal acceleration $\ddot{m}$ which changes $\dot{\overline{R}}$ (but, not $\overline{R}$). From Eq. (A41), we note that $\ddot{m}$ is caused by $\ddot{n}$ and the radial component of $\overline{\omega}_e$ (i.e., $\hat{r}\cdot\overline{\omega}_e$). For $\ddot{n}$ one may reflect the effects of any perturbation, e.g., the earth's oblateness with

$$\ddot{n} = -3J_2\frac{\mu_e}{r^2}\left(\frac{r_e}{r}\right)^2\frac{z}{r}\cos i \tag{A46}$$

where μ_e is the gravitational parameter of the earth, r_e is the mean radius of the equator, and J_2 is the second zonal harmonic of the geopotential. Again, for the purpose of state transformation, we can work with an osculating Keplerian orbit, i.e., we can set $\ddot{n} = 0$. Like $\ddot{n}$, $\hat{r}\cdot\overline{\omega}_e$ does not change $\{\overline{r},\dot{\overline{r}}\}$ and $\overline{R}$. However, the component of $\overline{\omega}_e$ normal to $\overline{r}$ changes $\dot{\overline{R}}$ and $\overline{R}$ as well as $\dot{\overline{r}}$ (but, not $\overline{r}$). We consider a simplified earth-rotation model uniformly rotating along the $\hat{e}_w$-axis, i.e.,

$$\overline{\omega}_e \approx \omega_o\hat{e}_w \approx \omega_o\hat{e}_z \tag{A47}$$

where ω_o represents the constant rate of the Greenwich mean sidereal time to be denoted by θ. Then, as the counterpart of Eq. (A16), the components of $\overline{R}$ can be expressed as

$$a = r^{1/2}\cos\tfrac{1}{2}(\vartheta+\tau)\cos\tfrac{1}{2}i, \quad b = r^{1/2}\cos\tfrac{1}{2}(\vartheta-\tau)\sin\tfrac{1}{2}i$$
$$c = r^{1/2}\sin\tfrac{1}{2}(\vartheta-\tau)\sin\tfrac{1}{2}i, \quad d = r^{1/2}\sin\tfrac{1}{2}(\vartheta+\tau)\cos\tfrac{1}{2}i \tag{A48}$$

where

$$\vartheta = \Omega - \theta \tag{A49}$$

is the argument of ascending orbital node measured from the Greenwich meridian.

References

Battin RH (1987) An introduction to the mathematical methods of astrodynamics. American Institute of Aeronautics and Astronautics, New York

Born GH, Tapley BD, Santee ML (1986) Orbit determination using dual crossing arc altimetry. Acta Astronaut 13–4:157–163

Cartan E (1981) The theory of spinors. Dover, New York

Cloutier JR (1983) A technique for reducing low-frequency, time-dependent errors present in network-type surveys. J Geophys Res 88:659–663

Colombo OC (1984) Altimetry, orbits and tides. NASA Technical Memorandum 86180, Goddard Space Flight Center

Cui C, Lelgemann D (1992) On cross-over differences of the radial orbital perturbations as functions of force model parameters. In: Geodesy and physics of the earth, International Union of Geodesy and Geophysics. Springer, Berlin Heidelberg New York

Deprit A, Elipe A, Ferrer S (1994) Linearization: Laplace vs. Stiefel. Celestial Mech Dyn Astron 58:151–201

Farless DL (1985) The application of periodic orbits to TOPEX mission design. AAS 85–301:13–36

Ferziger JH (1981) Numerical methods for engineering application. Wiley, New York

Gaspar P, Ogor F, Le Traon P-Y, Zanife O-Z (1994) Estimating the sea state bias of the TOPEX and POSEIDON altimeters from crossover differences. J Geophys Res 99:24981–24994

Goldstein H (1980) Classical mechanics (2nd edn) Addison-Wesley, Reading Mass

Grafarend EW, Lohse P (1991) The minimal distance mapping of the topographic surface onto the (reference) ellipsoid of revolution. Manuscr Geod 16:92–110

Greiner W (1994) Quantum mechanics, an introduction (3rd edn) Springer, Berlin Heidelberg New York

Guckenheimer G, Holmes P (1986) Nonlinear oscillations, dynamical systems, and bifurcations of vector fields. Springer, Berlin Heidelberg New York

Hagar H (1977) Computation of circular orbit ground trace intersections. Engineering Memorandum 315–29, Jet Propulsion Laboratory

Hestenes D (1983) Celestial mechanics with geometric algebra. Celestial Mech 30:151–170

Hestenes D, Lounesto P (1983) Geometry of spinor regularization. Celestial Mech 30:171–179

Hsu SK, Geli L (1995) The effect of introducing continuity conditions in the constrained sinusoidal crossover adjustment method to reduce satellite orbit errors. Geophys Res Lett 22:949–952

Kim MC (1993) Determination of high-resolution mean sea surface and marine gravity field using satellite altimetry. Ph.D Dissertation. Dept Aerospace Engineering and Engineering Mechanics, The University of Texas at Austin

King JC (1976) Quantization and symmetry in periodic coverage patterns with applications to earth observation. J Astronaut Sci 24:347–363

Klokocnik J, Wagner CA (1994) A test of GEM-T2 from GEOSAT crossovers using latitude lumped coefficients. Bull Geod 68:100–108

Kozel BJ (1995) Dual-satellite altimeter crossover measurements for precise orbit determination. Ph.D. Dissertation. Dept Aerospace Engineering and Engineering Mechanics, The University of Texas at Austin

Lambeck K (1988) Geophysical geodesy, the slow deformations of the earth. Oxford University Press, Oxford
Landau LD, Lifshitz EM (1977) Quantum mechanics (non-relativistic theory) (3rd edn) Pergamon Press, Oxford
Leick A (1995) GPS satellite surveying (2nd edn) Wiley, New York
Ma XC, Shum CK, Eanes RJ, Tapley BD (1994) Determination of ocean tides from the first year of TOPEX/POSEIDON altimeter measurements. J Geophys Res 99:24809–24820
Moore P, Ehlers S (1993) Orbital refinement of ERS-1 using dual crossover arc techniques with TOPEX/POSEIDON. Manuscr Geod 18:249–262
Moore P, Rothwell DA (1990) A study of gravitational and non-gravitational modeling errors in crossover differences. Manuscr Geod 15:187–206
Nerem RS (1995) Global mean sea level variations from TOPEX/POSEIDON altimeter data. Science 268:708–711
Parke ME, Stewart RH, Farless DL (1987) On the choice of orbits for an altimetric satellite to study ocean circulation and tides. J Geophys Res 92:11693–11707
Press WH, Teukolsky SA, Vetterling WT, Flannery BP (1992) Numerical recipes in FORTRAN (2nd edn) Cambridge University Press, Cambridge
Rowlands D (1981) The adjustment of SEASAT altimeter data on a global basis for geoid and sea surface height determination. Report No. 325, Dept Geodetic Science and Surveying, The Ohio State University
Sandwell DT, Milbert DG, Douglas BC (1986) Global nondynamic orbit improvement for altimeter satellites. J Geophys Res 91:9447–9451
Santee ML (1985) Orbit correction using dual satellite crossing arc theory. CSR-85-4, Center for Space Research, The University of Texas at Austin
Schrama EJO (1989) The role of orbit errors in processing of satellite altimeter data. Ph.D. Thesis, Delft University Press, Delft
Schutz BE, Tapley BD, Shum CK (1982) Evaluation of the SEASAT altimeter time tag bias. J Geophys Res 87:3239–3245
Shepperd SW (1978) Quatenion from rotation matrix. J Guidance Control 1:223–224
Shum CK (1982) Altimeter methods in satellite geodesy. Ph.D. Dissertation. The University of Texas at Austin
Shum CK, Zhang BH, Schutz BE, Tapley BD (1990a) Altimeter crossover methods for precision orbit determination and the mapping of geophysical parameters. J Astronaut Sci 38:355–368
Shum CK, Werner RA, Sandwell DT, Zhang BH, Nerem RS, Tapley BD (1990b) Variations of global mesoscale eddy energy observed from GEOSAT. J Geophys Res 95:17865–17876
Spoecker NT (1991) Crossover generation. Technical Report ERS-D-ADP-32601, DGFI Dept 1, Munich, Germany
Stiefel EL, Scheifele G (1971) Linear and regular celestial mechanics. Springer, Berlin Heidelberg New York
Stottlemyer BA (1996) Improvement of the Venusian topography model using dual satellite altimeter crossover data from Magellan and the Pioneer Venus orbiter. Technical Memorandum (CSR-TM-94-04), Center for Space Research, The University of Texas at Austin
Tai CK, Fu LL (1986) On crossover adjustment in satellite altimetry and its oceanographic implications. J Geophys Res 91:2549–2554
Tapley BD, Ries JC, Davis GW, Eanes RJ, Schutz BE, Shum CK, Watkins MM, Marshall JA, Nerem RS, Putney BH, Klosko SM, Luthcke SB, Pavlis D, Williamson RG, Zelensky NP (1994) Precision orbit determination for TOPEX/POSEIDON. J Geophys Res 99:24383–24404
Torge W (1991) Geodesy, an introduction (2nd edn) Walter de Gruyter, Berlin
Whittaker ET (1937) A treatise on the analytical dynamics of particles and rigid bodies; with an introduction to the problem of three bodies (4th edn) Cambridge Univ Press, Cambridge
Wisse E, Naeije MC, Scharroo R, Smith AJE, Vossepoel FC, Wakker KF (1995) Processing of ERS-1 and TOPEX/POSEIDON altimeter measurements. BCRS report 95-02, Delft University of Technology, Faculty of Aerospace Engineering, Section Space Research and Technology